

A new method based on adaptive volume constraint and stress penalty for stress-constrained topology optimization

Sheng Chu¹ · Liang Gao¹ · Mi Xiao¹  · Zhen Luo² · Hao Li¹ · Xin Gui¹

Received: 26 May 2017 / Revised: 17 July 2017 / Accepted: 30 August 2017 / Published online: 18 September 2017
© Springer-Verlag GmbH Germany 2017

Abstract This paper focuses on the stress-constrained topology optimization of minimizing the structural volume and compliance. A new method based on adaptive volume constraint and stress penalty is proposed. According to this method, the stress-constrained volume and compliance minimization topology optimization problem is transformed into two simple and related problems: a stress-penalty-based compliance minimization problem and a volume-decision problem. In the former problem, stress penalty is conducted and used to control the local stress level of the structure. To solve this problem, the parametric level set method with the compactly supported radial basis functions is adopted. Meanwhile, an adaptive adjusting scheme of the stress penalty factor is used to improve the control of the local stress level. To solve the volume-decision problem, a combination scheme of the interval search and local search is proposed. Numerical examples are used to test the proposed method. Results show the lightweight design, which meets the stress constraint and whose compliance is simultaneously optimized, can be obtained by the proposed method.

Keywords Stress-constrained topology optimization · Adaptive volume constraint · Stress penalty · Stress-penalty-based compliance minimization · Volume-decision

✉ Mi Xiao
xiaomi@hust.edu.cn

¹ State Key Laboratory of Digital Manufacturing Equipment and Technology, Huazhong University of Science and Technology, Wuhan 430074, China

² School of Mechanical and Mechatronic Engineering, The University of Technology Sydney, 15 Broadway, Ultimo, NSW 2007, Australia

1 Introduction

In recent years, as a challenging problem, the stress-based topology optimization has attracted great attention (Silva and Cardoso 2017; Rong et al. 2016; Lopes and Novotny 2016; Lee et al. 2016). The common approaches, which are used to deal with the stress-based topology optimization problem, can be classified into three categories: the local method, the global method and the regional or block aggregation technique (Deaton and Grandhi 2014). In the local method (Bendsøe and Sigmund 2003; Pereira et al. 2004; Bruggi and Venini 2008; Verbart et al. 2016), the control of the stress level is acted on each finite element in the design domain. The ε -relaxation and qp -relaxation are proposed by Cheng and Guo (1997) and Bruggi (2008) to handle the singularity phenomenon of stress-based topology optimization, respectively. However, due to a large number of finite element constraints, the local method has a low computational efficiency (Collet et al. 2016). The global method (Guilherme and Fonseca 2007; Qiu and Li 2010; Yoon 2014) utilizes a whole stress measurement under considering all the local stress levels, and therefore can effectively reduce the computational cost. Yang and Chen (1996) propose the global stress measurement method based on the Kresselmeier Steinhauser (KS) function. Duysinx and Sigmund (1998) propose the global stress measurement method based on the p -norm and the p -mean. The KS function is improved by Luo et al. (2013) through aggregating the active and the passive local stress constraints. Kiyono et al. (2016) propose a multi- p -norm formulation approach to further develop the global method. However, the global method cannot ensure the maximum stresses are indeed controlled locally (Deaton and Grandhi 2014; Guo et al. 2014) and solving the stress-based topology optimization problem may become unstable and parameter-dependent because of its highly nonlinear behavior (Collet et al. 2016). By the

combination of the local and global methods, the regional or block aggregation technique (Paris et al. 2010; Holmberg et al. 2013) is developed. In this technique, the design domain is divided into several sub-regions. The local method is performed in each sub-region, and the global method is used to combine all the stress constraints in different sub-regions into a whole stress control. However, in order to control the stress level of a structure, most of the existing stress-based topology optimization methods may greatly sacrifice some other structural performances (such as the compliance of the structure) if these performances are not considered in the optimization (Xia et al. 2012).

As a typical stress-based topology optimization problem, the stress-constrained topology optimization problem has gained many attentions. When the structural stress level is limited, how to deal with the structural volume is one of the key issues. Generally, in many stress-constrained topology optimization problems, the volume is usually predetermined and used as a fixed constraint (Sigmund 2001; Wang et al. 2003; Zhang et al. 2015). Namely, the fixed allowable amount of material is distributed to a design domain. Guo et al. (2011) deal with the stress-related problem through the level set method, in which the stiffness measure is included and a global stress constraint and a volume constraint are considered. Guo et al. (2014) investigate the stress-related topology optimization involving multi-phase materials, in which the compliance is considered as the objective function and both the global stress level and the volume are regarded as the constraints. De Leon et al. (2015) consider the stress-constrained topology optimization for compliant mechanism design, where the objective function is to minimize the displacement in the output port subject to a global stress constraint and a volume constraint. However, in the stress-constrained topology optimization, because the set of the volume constraint is primarily dependent on the subjective experience of designers, the volume constraint easily leads to the violation of stress constraints (De Leon et al. 2015). Additionally, it may cause either an over- or under-design, even though the peak stress of the structure and compliance have been minimized (Lin and Sheu 2009). On the other hand, the structural volume can be viewed as the objective function in the stress-constrained topology optimization, namely the stress-constrained volume minimization problem. Jr Emmendoerfer and Fancello (2014) solve the problem of minimum mass with local stress constraints using the level set method. Jeong et al. (2014) proposed a novel phase-field method for stress-based shape and topology optimization method, where the volume is minimized and the local stress constraints are involved. Nevertheless, it is pointed out that the use of the volume as the objective function in the stress-constrained topology optimization may lower other structural performances (such as the stiffness) if these performances are not considered in the optimization (Lin and Sheu 2009). To

address the aforementioned issues, Collet et al. (2016) propose an approach aiming at the minimization of the structural volume under the local fatigue constraints along with a global enforcement on the overall compliance. Lin and Sheu (2009) propose an adaptive volume constraint (AVC) algorithm for the stress limit-based topology optimization. In this algorithm, the amount of material during optimization is adjusted to satisfy the maximum stress limit while simultaneously minimizing the compliance. The sensitivity analysis of stress constraints is avoided in this algorithm and the computational cost is drastically reduced. However, the structural stress level is actually not optimized in the AVC algorithm.

This paper focuses on the stress-constrained topology optimization of minimizing the structural volume and compliance, namely the volume-compliance minimization. A lightweight structure that meets the stress constraint is expected to be obtained and its compliance is simultaneously optimized to exclude the pathological structures with small stiffness. A new method based on AVC and stress penalty is proposed. According to this method, the stress-constrained volume-compliance minimization problem is transformed into two simple and related problems: a stress-penalty-based compliance minimization problem and a volume-decision problem. In the former problem, stress penalty is employed to control the local stress level of the structure. Specifically, to achieve the stress penalty, only the regions where the stresses are larger than the allowable stress will be considered and its corresponding stress level will be optimized. To solve the optimization problem, the parametric level set method (PLSM) with the compactly supported radial basis functions (CSRBFs) (Luo et al. 2007; Luo et al. 2008) is employed. Additionally, an adaptive adjusting scheme of the stress penalty factor is applied to improve the control of the local stress level. For the volume-decision problem, a combination scheme of the interval search and local search is proposed to determine a suitable volume fraction limit by comparing the structural maximum stress and the allowable stress.

The remainder of this paper is organized as follows. In Section 2, the formulation of stress-constrained topology optimization of minimizing the structural volume-compliance by using the proposed method based on AVC and stress penalty is provided, and how to solve the stress-penalty-based compliance minimization problem and the volume-decision problem is elaborated. Section 3 takes some numerical examples to test the proposed method. Conclusions are given in Section 4.

2 Stress-constrained topology optimization of minimizing the structural volume-compliance

To obtain a lightweight structure that meets the stress constraint and whose compliance is simultaneously optimized, the corresponding stress-constrained volume-compliance

minimization topology optimization problem can be formulated as (1) according to the PLSM based on the CSRBFs.

$$\begin{aligned} \min F &= [G(\Phi), J(\mathbf{u}, \Phi)]^T \\ \text{s.t. } a(\mathbf{u}, \mathbf{v}, \Phi) &= l(\mathbf{v}, \Phi), \mathbf{u}|_{\partial\Omega} = \mathbf{u}_0, \forall \mathbf{v} \in \mathbf{U} \\ \zeta \bar{\sigma} &\leq \sigma_{v, \max} \leq \bar{\sigma} \\ \beta_{i, \min} &\leq \beta_i \leq \beta_{i, \max} \end{aligned} \tag{1}$$

where $G(\Phi)$ is the volume of the structure and $J(\mathbf{u}, \Phi)$ is the compliance measurement. \mathbf{u} and \mathbf{v} denote the real displacement field and the virtual displacement field, respectively. \mathbf{U} is the space of kinematically admissible displacement fields. $\mathbf{u}|_{\partial\Omega} = \mathbf{u}_0$ denotes the displacement constraint on the structural boundary. Φ is the level set function and $\Phi = \boldsymbol{\varphi} \boldsymbol{\beta}$ in the PLSM, where $\boldsymbol{\varphi}$ is the matrix of the shape function of the CSRBFs and $\boldsymbol{\beta}$ is the vector of the design variable β_i . β_i is the expansion coefficient at the i th knot in the PLSM. σ_v and $\bar{\sigma}$ are the von Mises stress and the allowable stress, respectively. ζ is the tolerance factor. The structural maximum stress $\sigma_{v, \max}$ is expected to be near $\bar{\sigma}$ to make good use of materials and reduce the use of materials. $\beta_{i, \min}$ and $\beta_{i, \max}$ are the lower and upper bounds of the design variable. The state equation for the elastic continuum structures is given in the weak form of $a(\mathbf{u}, \mathbf{v}, \Phi) = l(\mathbf{v}, \Phi)$. The bilinear function $a(\mathbf{u}, \mathbf{v}, \Phi)$ and the bilinear operator $l(\mathbf{v}, \Phi)$ are defined as:

$$a(\mathbf{u}, \mathbf{v}, \Phi) = \int_{\Omega} \boldsymbol{\varepsilon}^T(\mathbf{u}) \mathbf{D} \boldsymbol{\varepsilon}(\mathbf{v}) H(\Phi) d\Omega \tag{2}$$

$$l(\mathbf{v}, \Phi) = \int_{\Omega} \mathbf{p} \mathbf{v} H(\Phi) d\Omega + \int_{\Omega} \boldsymbol{\tau} \mathbf{v} \delta(\Phi) |\nabla \Phi| d\Omega \tag{3}$$

where $\boldsymbol{\varepsilon}$ stands for the strain field, and \mathbf{D} denotes the elastic stiffness. \mathbf{p} and $\boldsymbol{\tau}$ are the structural volume force and boundary traction, respectively. $H(\Phi)$ is the Heaviside function (Wang et al. 2003; Allaire et al. 2004). $\delta(x)$ is the Dirac function, namely the derivative of the Heaviside function. In this paper, the following smoothed approximation of the Heaviside function $H(x)$ and the Dirac function $\delta(x)$ are used (Wang et al. 2003).

$$H(x) = \begin{cases} 0 & x < -\Delta \\ \frac{3(1-\mu)}{4} \left(\frac{x}{\Delta} - \frac{x^3}{3\Delta^3} \right) + \frac{1+\mu}{2} & -\Delta \leq x < \Delta \\ 1 & x \geq \Delta \end{cases} \tag{4}$$

$$\delta(x) = \begin{cases} \frac{3(1-\mu)}{4\Delta} \left(1 - \frac{x^2}{\Delta^2} \right) & |x| \leq \Delta \\ \gamma & |x| > \Delta \end{cases} \tag{5}$$

where Δ is the different value which is used to describe the width of numerical approximation. Both μ and γ are small positive numbers to avoid singularity.

According to the method based on AVC and stress penalty, the stress-constrained volume-compliance minimization problem in (1) is transformed into two simple and related problems: the stress-penalty-based compliance minimization

problem and a volume-decision problem. In the former problem, the stress penalty is conducted and considered in the objective function. The compliance and the stress level are optimized simultaneously under the volume constraint. Meanwhile, the volume fraction limit will be determined and adjusted by solving the volume-decision problem to control the structural volume. Specifically, an initial volume fraction limit is predetermined. After solving the stress-penalty-based compliance minimization problem, an optimal structure can be obtained. Then, in the volume-decision problem, after the comparison of the maximum stress of the current optimal structure and the allowable stress, the volume fraction limit is adjusted by a certain method. The adjusted volume fraction limit will be transferred back to the stress-penalty-based compliance minimization problem. The above solving process will be repeated until the optimal lightweight design is obtained, which meets the stress constraint and whose compliance is simultaneously optimized. The details of the stress-penalty-based compliance minimization problem, the volume-decision problem and the whole solving process will be elaborated in the following sections.

2.1 Stress-penalty-based compliance minimization topology optimization

2.1.1 Problem formulation

According to the PLSM based on the CSRBFs, the stress-penalty-based compliance minimization problem can be formulated as follows:

$$\begin{aligned} \min \bar{J}(\mathbf{u}, \Phi) &= \int_{\Omega} \frac{1}{2} \boldsymbol{\varepsilon}^T(\mathbf{u}) \mathbf{D} \boldsymbol{\varepsilon}(\mathbf{u}) \left(1 + \alpha H_{obj}(\sigma_v - \bar{\sigma}) \right) H(\Phi) d\Omega \\ \text{s.t. } a(\mathbf{u}, \mathbf{v}, \Phi) &= l(\mathbf{v}, \Phi), \mathbf{u}|_{\partial\Omega} = \mathbf{u}_0, \forall \mathbf{v} \in \mathbf{U} \\ G(\Phi) &= \int_{\Omega} H(\Phi) d\Omega \leq \bar{V} \int_{\Omega} d\Omega \\ \beta_{i, \min} &\leq \beta_i \leq \beta_{i, \max} \end{aligned} \tag{6}$$

where $\bar{J}(\mathbf{u}, \Phi)$ is objective function of the stress-penalty-based compliance minimization problem, and α is a stress penalty factor. \bar{V} is the volume fraction limit and will be adjusted by solving the volume-decision problem to control the structural volume, which will be discussed in Section 2.2.

From (6), it can be seen that the objective function consists of two parts: the compliance and a penalty of the stress which is larger than the allowable stress. Although this way of controlling the stress level by the objective function instead of the constraint belongs to the local method mentioned in the Introduction Section, it can avoid the huge computational burden due to a large number of stress constraints in the existing local methods. The stress penalty factor α controls the weight of the penalization, which is of vital importance for controlling the maximum stress because it makes the stress that is

larger than the allowable stress play a prominent role during the optimization. Specifically, only the structure in the region where the corresponding stress is more than the allowable stress will be optimized by the penalty of the stresses in the objective function. Accordingly, the local stress level of the whole structure is controlled. To make the objective function and its sensitivity differentiable and continuous, the Heaviside function is introduced. The approximate Heaviside function $H_{obj}(\cdot)$ and its derivative $\delta_{obj}(\cdot)$ are defined as

$$H_{obj}(x) = \begin{cases} 0 & x < -\Delta_{obj} \\ \frac{3}{4} \left(\frac{x}{\Delta} - \frac{x^3}{3\Delta^3} \right) + \frac{1}{2} & -\Delta_{obj} \leq x < \Delta_{obj} \\ 1 & x \geq \Delta_{obj} \end{cases} \quad (7)$$

$$\delta_{obj}(x) = \begin{cases} \frac{3}{4\Delta} \left(1 - \frac{x^2}{\Delta^2} \right) & |x| \leq \Delta_{obj} \\ 0 & |x| > \Delta_{obj} \end{cases} \quad (8)$$

where Δ_{obj} is the different value in $H_{obj}(\sigma_v - \bar{\sigma})$ for controlling the local stress level. When Δ_{obj} increases, the band of transition becomes wider and smoother. However, it causes that the penalization will be conducted when $\sigma_v > \bar{\sigma} - \Delta_{obj}$.

2.1.2 Sensitivity analysis

In this paper, the optimality criteria (OC) method (Bendsøe 1995; Sigmund 2001), which is a gradient-based method, is used to solve the stress-penalty-based compliance minimization problem in (6). The sensitivity analysis for this problem is required and described in this section.

For convenience of description, it is set that $\mathbf{k}_e = \mathbf{B}^T \mathbf{D} \mathbf{B}$ and $\mathbf{C}_e = \mathbf{B}^T \mathbf{D}^T \mathbf{V} \mathbf{D} \mathbf{B}$, where \mathbf{B} is the strain-displacement matrix and \mathbf{V} is an auxiliary matrix and used to solve the von Mises stress and estimate plane stress, which is given by

$$\mathbf{V} = \begin{bmatrix} 1 & -\frac{1}{2} & 0 \\ -\frac{1}{2} & 1 & 0 \\ 0 & 0 & 3 \end{bmatrix} \quad (9)$$

Then the objective function in (6) and the bilinear function in (2) can be rewritten as

$$\begin{aligned} \bar{J}(\mathbf{u}, \Phi) &= \int_{\Omega} \frac{1}{2} \mathbf{u}^T \mathbf{B}^T \mathbf{D} \mathbf{B} \mathbf{u} \left(1 + \alpha H_{obj}(\sigma_v - \bar{\sigma}) \right) H(\Phi) d\Omega \\ &= \int_{\Omega} \frac{1}{2} \mathbf{u}^T \mathbf{k}_e \mathbf{u} \left(1 + \alpha H_{obj}(\sigma_v - \bar{\sigma}) \right) H(\Phi) d\Omega \end{aligned} \quad (10)$$

$$a(\mathbf{u}, \mathbf{v}, \Phi) = \int_{\Omega} \mathbf{u}^T \mathbf{B}^T \mathbf{D} \mathbf{B} \mathbf{v} H(\Phi) d\Omega = \int_{\Omega} \mathbf{u}^T \mathbf{k}_e \mathbf{v} H(\Phi) d\Omega \quad (11)$$

where $H_{obj}(\sigma_v - \bar{\sigma})$ can be simplified to $H_{obj}(\left(\mathbf{u}^T \mathbf{C}_e \mathbf{u}\right)^{1/2} - \bar{\sigma})$ through the PLSM and the relaxation method based on the stress (Duysinx and Bendsøe 1998).

In this section, the shape derivative (Choi and Kim 2005; Haug et al. 1986; Wang and Wang 2004) and the adjoint method are employed. The Lagrangian is defined as

$$\Psi = \bar{J}(\mathbf{u}, \Phi) + a(\mathbf{u}, \mathbf{v}, \Phi) - l(\mathbf{v}, \Phi) + \lambda \left(G(\Phi) - \bar{V} \int_{\Omega} d\Omega \right) \quad (12)$$

where λ is a Lagrangian multiplier for the volume constraint. According to the linearity of the admissible displacement field, $a(\mathbf{u}, \mathbf{v}, \Phi) = l(\mathbf{v}, \Phi)$ and it is regarded as an Equation for solving the displacement field rather than defining a constraint. The shape derivative of the Lagrangian over the time is shown by

$$\frac{\partial \Psi}{\partial t} = \frac{\partial \bar{J}(\mathbf{u}, \Phi)}{\partial t} + \frac{\partial a(\mathbf{u}, \mathbf{v}, \Phi)}{\partial t} - \frac{\partial l(\mathbf{v}, \Phi)}{\partial t} + \lambda \frac{\partial G(\Phi)}{\partial t} \quad (13)$$

where the derivatives $\frac{\partial \bar{J}(\mathbf{u}, \Phi)}{\partial t}$, $\frac{\partial a(\mathbf{u}, \mathbf{v}, \Phi)}{\partial t}$, $\frac{\partial l(\mathbf{v}, \Phi)}{\partial t}$ and $\frac{\partial G(\Phi)}{\partial t}$ are given by

$$\begin{aligned} \frac{\partial \bar{J}(\mathbf{u}, \Phi)}{\partial t} &= \int_{\Omega} \dot{\mathbf{u}}^T \mathbf{k}_e \mathbf{u} \left(1 + \alpha H_{obj} \left(\left(\mathbf{u}^T \mathbf{C}_e \mathbf{u} \right)^{1/2} - \bar{\sigma} \right) \right) H(\Phi) d\Omega \\ &\quad + \int_{\Omega} \mathbf{u}^T \mathbf{k}_e \alpha \delta_{obj} \left(\left(\mathbf{u}^T \mathbf{C}_e \mathbf{u} \right)^{1/2} - \bar{\sigma} \right) \left(\frac{1}{2} \left(\mathbf{u}^T \mathbf{C}_e \mathbf{u} \right)^{-1/2} \dot{\mathbf{u}}^T \mathbf{C}_e \mathbf{u} \right) H(\Phi) d\Omega \\ &\quad + \int_{\Omega} \frac{1}{2} \mathbf{u}^T \mathbf{k}_e \mathbf{u} \left(1 + \alpha H_{obj} \left(\left(\mathbf{u}^T \mathbf{C}_e \mathbf{u} \right)^{1/2} - \bar{\sigma} \right) \right) \delta(\Phi) \frac{\partial \Phi}{\partial t} d\Omega \end{aligned} \quad (14)$$

$$\begin{aligned} \frac{\partial a(\mathbf{u}, \mathbf{v}, \Phi)}{\partial t} &= \int_{\Omega} \dot{\mathbf{u}}^T \mathbf{k}_e \mathbf{v} H(\Phi) d\Omega + \int_{\Omega} \mathbf{u}^T \mathbf{k}_e \dot{\mathbf{v}} H(\Phi) d\Omega \\ &\quad + \int_{\Omega} \mathbf{u}^T \mathbf{k}_e \mathbf{v} \delta(\Phi) \frac{\partial \Phi}{\partial t} d\Omega \end{aligned} \quad (15)$$

$$\begin{aligned} \frac{\partial l(\mathbf{v}, \Phi)}{\partial t} &= \int_{\Omega} (\mathbf{p} \dot{\mathbf{v}} + \text{div}(\boldsymbol{\tau} \mathbf{v})) d\Omega \\ &\quad + \int_{\Omega} (\mathbf{p} \mathbf{v} + \text{div}(\boldsymbol{\tau} \mathbf{v})) \delta(\Phi) \frac{\partial \Phi}{\partial t} d\Omega \end{aligned} \quad (16)$$

$$\frac{\partial G(\Phi)}{\partial t} = \int_{\Omega} \delta(\Phi) \frac{\partial \Phi}{\partial t} d\Omega \quad (17)$$

The weak form of the state equation can be obtained by collecting all the terms that contain $\dot{\mathbf{v}}$ on the right side of (13) and making their sum to be zero, that is

$$\int_{\Omega} \mathbf{u}^T \mathbf{k}_e \dot{\mathbf{v}} H(\Phi) d\Omega = \int_{\Omega} (\mathbf{p} \dot{\mathbf{v}} + \text{div}(\boldsymbol{\tau} \mathbf{v})) d\Omega \quad (18)$$

The adjoint equation, which is used to solve \mathbf{v} , can be obtained by collecting all the terms that include $\dot{\mathbf{u}}$ on the right side of (13) and letting their sum to be zero, that is

$$\begin{aligned} \int_{\Omega} \dot{\mathbf{u}}^T \mathbf{k}_e \mathbf{v} H(\Phi) d\Omega + \int_{\Omega} \dot{\mathbf{u}}^T \mathbf{k}_e \mathbf{u} \left(1 + \alpha H_{obj} \left(\left(\mathbf{u}^T \mathbf{C}_e \mathbf{u} \right)^{1/2} - \bar{\sigma} \right) \right) H(\Phi) d\Omega + \\ \int_{\Omega} \mathbf{u}^T \mathbf{k}_e \alpha \delta_{obj} \left(\left(\mathbf{u}^T \mathbf{C}_e \mathbf{u} \right)^{1/2} - \bar{\sigma} \right) \left(\frac{1}{2} \left(\mathbf{u}^T \mathbf{C}_e \mathbf{u} \right)^{-1/2} \dot{\mathbf{u}}^T \mathbf{C}_e \mathbf{u} \right) H(\Phi) d\Omega = 0 \end{aligned} \quad (19)$$

Ignoring the body force and noticing that only boundaries based on the homogeneous Neumann boundary condition subject to optimization (Xia et al. 2012), the shape derivative of the Lagrangian can be gained by substituting (18) and (19) into (13), that is

$$\frac{\partial \Psi}{\partial t} = \int_{\Omega} \frac{1}{2} \mathbf{u}^T \mathbf{k}_e \mathbf{u} \left(1 + \alpha H_{obj} \left((\mathbf{u}^T \mathbf{C}_e \mathbf{u})^{1/2} - \bar{\sigma} \right) \right) \delta(\Phi) \frac{\partial \Phi}{\partial t} d\Omega + \int_{\Omega} \mathbf{u}^T \mathbf{k}_e \mathbf{v} \delta(\Phi) \frac{\partial \Phi}{\partial t} d\Omega + \lambda \int_{\Omega} \delta(\Phi) \frac{\partial \Phi}{\partial t} d\Omega \quad (20)$$

Using the CSRBFs $\Phi(x, t) = \varphi(x)\beta(t)$, (20) can be rewritten as

$$\frac{\partial \Psi}{\partial t} = \sum_{i=1}^N \int_{\Omega} \gamma(\mathbf{u}, \mathbf{v}, \Phi) \varphi_i(x) \delta(\Phi) \frac{d\beta_i(t)}{dt} d\Omega \quad (21)$$

where $\varphi_i(x)$ is the shape function of the CSRBFs, and $\gamma(\mathbf{u}, \mathbf{v}, \Phi)$ is given by

$$\gamma(\mathbf{u}, \mathbf{v}, \Phi) = \frac{1}{2} \mathbf{u}^T \mathbf{k}_e \mathbf{u} \left(1 + \alpha H_{obj} \left((\mathbf{u}^T \mathbf{C}_e \mathbf{u})^{1/2} - \bar{\sigma} \right) \right) + \mathbf{u}^T \mathbf{k}_e \mathbf{v} + \lambda \quad (22)$$

The above equation can be expanded as

$$\frac{\partial \Psi}{\partial t} = \sum_{i=1}^N \gamma_1^T \frac{d\beta_i(t)}{dt} + \sum_{i=1}^N \gamma_2^T \frac{d\beta_i(t)}{dt} \quad (23)$$

where γ_1 and γ_2 are defined as:

$$\gamma_1 = \int_{\Omega} \left(\frac{1}{2} \mathbf{u}^T \mathbf{k}_e \mathbf{u} \left(1 + \alpha H_{obj} \left((\mathbf{u}^T \mathbf{C}_e \mathbf{u})^{1/2} - \bar{\sigma} \right) \right) + \mathbf{u}^T \mathbf{k}_e \mathbf{v} \right) \varphi_i(x) \delta(\Phi) d\Omega \quad (24)$$

$$\gamma_2 = \lambda \int_{\Omega} \varphi_i(x) \delta(\Phi) d\Omega \quad (25)$$

On the other hand, the shape derivative of the Lagrangian can be obtained by using the chain rule, that is

$$\frac{\partial \Psi}{\partial t} = \left(\sum_{i=1}^N \frac{\partial \bar{J}(\mathbf{u}, \Phi)}{\partial \beta_i(t)} + \lambda \sum_{i=1}^N \frac{\partial (G(\Phi) - \bar{V} \int_{\Omega} d\Omega)}{\partial \beta_i(t)} \right) \frac{d\beta_i(t)}{dt} \quad (26)$$

Then the design sensitivity for the objective function and the volume constraint can be obtained by comparing the corresponding terms in (23) and (26), that is

$$\frac{\partial \bar{J}(\mathbf{u}, \Phi)}{\partial \beta_i(t)} = \int_{\Omega} \left(\frac{1}{2} \mathbf{u}^T \mathbf{k}_e \mathbf{u} \left(1 + \alpha H_{obj} \left((\mathbf{u}^T \mathbf{C}_e \mathbf{u})^{1/2} - \bar{\sigma} \right) \right) + \mathbf{u}^T \mathbf{k}_e \mathbf{v} \right) \varphi_i(x) \delta(\Phi) d\Omega \quad (27)$$

$$\frac{\partial (G(\Phi) - \bar{V} \int_{\Omega} d\Omega)}{\partial \beta_i(t)} = \int_{\Omega} \varphi_i(x) \delta(\Phi) d\Omega \quad (28)$$

Finally, the stress-penalty-based compliance minimization problem in (6) can be solved via the gradient based method. The OC method and the bisection method are used to update the design variables $\beta_i(t)$ and the Lagrange multiplier λ in this paper, respectively. It is worth noting that the OC method and its related KKT conditions used in this manuscript are similar to those utilized in the work by Luo et al. (2008). A brief introduction about them will be given in Section 2.3.4. Additionally, the terminal condition for the stress-penalty-based compliance minimization problem is given by

$$\left| \frac{\bar{J}^k - \bar{J}^{k-1}}{\bar{J}^{k-1}} \right| < \xi \quad \& \quad \left| \frac{\sigma_{v,max}^k - \sigma_{v,max}^{k-1}}{\sigma_{v,max}^{k-1}} \right| < \zeta \quad (29)$$

where \bar{J}^k and $\sigma_{v,max}^k$ are the values of the objective function and maximum stress of the optimal structure after k th iterations, respectively. Both ξ and ζ are a small positive number.

2.2 Combination scheme for volume-decision

The volume-decision problem is shown in (30). In this problem, the volume fraction limit will be determined and transferred to the stress-penalty-based compliance minimization problem in (6) in order to obtain a lightweight design.

$$\min \bar{V} \quad (30) \\ s.t. \quad \zeta \bar{\sigma} \leq \sigma_{v,max} \leq \bar{\sigma}$$

The volume-decision problem is solved by the means of automatically modifying the volume fraction limit after comparing the structural maximum stress $\sigma_{v,max}$ and the allowable stress $\bar{\sigma}$. In this paper, a combination scheme of the interval search and local search is proposed to determine a suitable volume fraction limit. Specifically, the interval search scheme is used to narrow the search range of the feasible volume fraction limit and find a suitable volume fraction limit interval, in which the local search scheme is utilized to find the final volume fraction limit. The detailed introduction of the two methods will be provided in the following sections.

2.2.1 Interval search scheme

In this paper, the interval search step is set to 0.1, which can ensure the obvious changes of the structure and its maximum

stress after each change of the volume constraint. The volume fraction limit is changed according to the following scheme:

$$\bar{V}^{i+1} = \begin{cases} \bar{V}^i + 0.1, & \sigma_{v,\max}^i > \bar{\sigma} \\ \bar{V}^i - 0.1, & \sigma_{v,\max}^i \leq \bar{\sigma} \end{cases} \quad (31)$$

where $\sigma_{v,\max}^i$ is the maximum stress of the optimal structure with \bar{V}^i after the i th change of the volume constraint.

In order to gain a suitable volume fraction interval and further determine the final volume fraction limit, the terminal condition of the interval search scheme is set as

$$\begin{cases} \bar{\sigma} \in [\sigma_{v,\max}^{i-1}, \sigma_{v,\max}^i], \bar{V}^{i-1} > \bar{V}^i \\ \bar{\sigma} \in [\sigma_{v,\max}^i, \sigma_{v,\max}^{i-1}], \bar{V}^{i-1} \leq \bar{V}^i \end{cases} \quad (32)$$

When the terminal condition is satisfied, the suitable volume fraction interval will be obtained. But it is worth noting that the volume fraction interval obtained is $[0, \max(\bar{V}^{i-1}, \bar{V}^i)]$ or $[\min(\bar{V}^{i-1}, \bar{V}^i), 1]$ rather than $[\bar{V}^{i-1}, \bar{V}^i]$. This is because the maximum number of iteration after each change of the volume constraint is set in the optimization to prevent too much iterations. The final structure with the volume fraction limit \bar{V}^i may be not the corresponding optimal structure, and its maximum stress may be smaller or bigger. Thus, the final volume fraction limit can merely be determined as $[0, \max(\bar{V}^{i-1}, \bar{V}^i)]$ when $\bar{V}^{i-1} > \bar{V}^i$, or $[\min(\bar{V}^{i-1}, \bar{V}^i), 1]$ when $\bar{V}^{i-1} \leq \bar{V}^i$.

2.2.2 Local search scheme

For the local search scheme, the volume fraction limit is changed according to the following scheme:

$$\bar{V}^{j+1} = \begin{cases} \bar{V}^j + \min\left(1.25 \times \bar{V}^0 \times \left|\frac{\sigma_{v,\max}^j - \bar{\sigma}}{\bar{\sigma}}\right|, \max\left(\frac{0.1}{2^j}, 0.002\right)\right), & \sigma_{v,\max}^j > \bar{\sigma} \\ \bar{V}^j - \min\left(1.25 \times \bar{V}^0 \times \left|\frac{\sigma_{v,\max}^j - \bar{\sigma}}{\bar{\sigma}}\right|, \max\left(\frac{0.1}{2^j}, 0.002\right)\right), & \sigma_{v,\max}^j \leq \bar{\sigma} \end{cases} \quad (33)$$

where j denotes the j th change of the volume constraint after the local search scheme is conducted. From (33), it can be seen that the change of the volume constraint is related to the initial volume constraint of the whole optimization and the relative deviation between the current maximum stress and the allowable stress. Near the end of the optimization, the maximum

stress is approaching the target value and the term $1.25 \times \bar{V}^0 \times \left|\frac{\sigma_{v,\max}^j - \bar{\sigma}}{\bar{\sigma}}\right|$ dominates the change of the volume constraint. The maximum change of the volume constraint is limited and gradually changed by the bisection method (Kaw et al. 2011). The constant 0.002 is set to avoid a small change of the volume constraint because a slight change of the structure and its maximum stress will cause more optimization iterations to obtain the final topological structure.

To obtain the lightweight structure which meets the stress constraint, the terminal condition of the local search scheme is set as (34). It is also used as the termination judgment for the stress-constrained topology optimization with AVC and stress penalty.

$$\varsigma \bar{\sigma} \leq \sigma_{v,\max} \leq \bar{\sigma} \quad (34)$$

2.3 Numerical implementation

2.3.1 Adaptive adjusting scheme of the stress penalty factor

The stress penalty factor α in (6) has a significant effect on the topology optimization results. If the stress penalty factor is set too small, it will be difficult to effectively control the local stress level. And the structural maximum stress may be larger than the allowable stress and the volume fraction limit will be increased, which can easily lead to a local optimum. On the contrary, if the stress penalty factor is set too large, the optimization will become unstable due to the abrupt change of the objective function during the optimization. In this paper, an adaptive scheme is used to adjust the value of the stress penalty factor. When the maximum stress keeps stable and the stress constraint is still not satisfied, the stress penalty factor will be increased. It is defined as

$$\alpha = \alpha + 1, \text{ if } \left(\frac{\sigma_{v,\max}^k - \sigma_{v,\max}^{k-1}}{\sigma_{v,\max}^{k-1}}\right) \leq \xi \& \left(\frac{\sigma_{v,\max}^k - \sigma_{v,\max}^{k-2}}{\sigma_{v,\max}^{k-2}}\right) \leq \xi \& \sigma_{v,\max}^k > \bar{\sigma} \quad (35)$$

where $\sigma_{v,\max}^k$ is the maximum stress of the optimal structure after k th iterations.

2.3.2 Compactly supported radial basis function

In this paper, the following CSRBF with C2 smoothness (Luo et al. 2008; Wendland 1995) is applied in the PLSM

$$\varphi_i(x) = \max\left\{0, (1-r_i(x))^4\right\} (4r_i(x) + 1) \quad (36)$$

where r is the radius of support and usually defined in a 2D Euclidean space by

$$r_i(x) = \frac{\sqrt{(x-x_i)^2 + (y-y_i)^2}}{d_{ml}} \tag{37}$$

where $d_{ml} = 3.5$ in this paper.

2.3.3 Finite element method

As in most topology optimization methods, the finite element method (FEM) with structured four-node bi-linear elements is employed in the displacement analysis to enhance the computational efficiency, and the ersatz material model is adopted for FEM analysis (Zhang et al. 2015; Wang et al. 2015). Therefore, the Young’s modulus of the e^{th} element can be interpolated by

$$D_e = \left[\frac{1}{V_e} \int_{\Omega_e} H(\Phi) d\Omega \right] D, e = 1, 2, \dots, n \tag{38}$$

where Ω_e represents the region covered by the e^{th} element, V_e is the area of the e^{th} element and n is the number of the elements. $\left[\frac{1}{V_e} \int_{\Omega_e} H(\Phi) d\Omega \right]$ can be regarded as the density of the e^{th} element.

In order to calculate the equivalent stress for the artificial weak material around the boundary, the following stress criterion (Duysinx and Bendsøe 1998) is applied.

$$\langle \sigma \rangle = \frac{\sigma_v}{\rho^q} = \frac{\rho^p}{\rho^q} (u^T C_e u)^{1/2} \tag{39}$$

where $\langle \sigma \rangle$ is the equivalent stress for the ersatz material model, ρ is the density of the element, p is the penalty factor of the density and q is the penalty factor for the equivalent stress. According to the work by Choi and Kim (2005), $p = q$.

It is worth noting that the X-FEM approaches (Guo et al. 2016) and body-fitted adaptive mesh techniques (Liu and Korvink 2008) can be employed in the proposed method to remove the artificial weak material and further improve the accuracy of the stress calculation since the clear boundaries of the structure can be explicitly described in the PLSM.

2.3.4 Optimality criteria method

In order to solve the stress-penalty-based compliance minimization problem shown in Section 2.1, the OC method is applied. For the optimization problem in (6), after introducing

Lagrange multipliers λ_1 and λ_2 , the Lagrangian Ψ is reconstructed as

$$\Psi = \bar{J}(\mathbf{u}, \Phi) + \lambda \left(G(\Phi) - \bar{V} \int_{\Omega} d\Omega \right) + \lambda_1 (\beta_{i,\min} - \beta_i) + \lambda_2 (\beta_i - \beta_{i,\max}) \tag{40}$$

The Kuhn-Tucker conditions can be obtained according to its stationary conditions:

$$\begin{cases} \frac{\partial \bar{J}(\mathbf{u}, \Phi)}{\partial \beta_i(t)} + \lambda \frac{\partial (G(\Phi) - \bar{V} \int_{\Omega} d\Omega)}{\partial \beta_i(t)} - \lambda_1 + \lambda_2 \\ = \begin{cases} = 0 & \text{if } \beta_{i,\min} \leq \beta_i \leq \beta_{i,\max} \\ \geq 0 & \text{if } \beta_i < \beta_{i,\min} \\ \leq 0 & \text{if } \beta_i > \beta_{i,\max} \end{cases} \\ \begin{cases} G(\Phi) - \bar{V} \int_{\Omega} d\Omega \leq 0 \\ \lambda (G(\Phi) - \bar{V} \int_{\Omega} d\Omega) = 0, \quad \lambda \geq 0 \\ \beta_{i,\min} - \beta_i \leq 0 \\ \lambda_1 (\beta_{i,\min} - \beta_i) = 0, \quad \lambda_1 \geq 0 \\ \beta_i - \beta_{i,\max} \leq 0 \\ \lambda_2 (\beta_i - \beta_{i,\max}) = 0, \quad \lambda_2 \geq 0 \end{cases} \end{cases} \tag{41}$$

Assuming that the design variables are active, the stationary condition is again given as follows

$$\begin{cases} \frac{\partial \bar{J}(\mathbf{u}, \Phi)}{\partial \beta_i(t)} + \lambda \frac{\partial (G(\Phi) - \bar{V} \int_{\Omega} d\Omega)}{\partial \beta_i(t)} = 0 \\ \begin{cases} G(\Phi) - \bar{V} \int_{\Omega} d\Omega \leq 0 \\ \lambda (G(\Phi) - \bar{V} \int_{\Omega} d\Omega) = 0, \quad \lambda \geq 0 \end{cases} \end{cases} \tag{42}$$

Then an efficient heuristic updating scheme based on the Kuhn-Tucker conditions is applied (Luo et al. 2008). Its iteration pattern for the design variables is designed as

$$\beta_i^{(k+1)} = D_i^{(k)} \beta_i^{(k)} \tag{43}$$

where $\beta_i^{(k)}$ is the design valuable at k th iteration and $D_i^{(k)}$ is defined as

$$D_i^{(k)} = \frac{\partial \bar{J}(\mathbf{u}, \Phi)}{\partial \beta_i^{(k)}(t)} / \left(\max \left(\mu, \lambda^{(k)} \frac{\partial (G(\Phi) - \bar{V} \int_{\Omega} d\Omega)}{\partial \beta_i^{(k)}(t)} \right) \right) \tag{44}$$

where μ is a very small positive constant and used to remove the zero terms. The design sensitivities are shown in (27) and (28). The following scheme is given by considering the lateral constraints

$$\beta_{\min}^{(k)} \leq \beta^{(k+1)} \leq \beta_{\max}^{(k)} \tag{45}$$

where $\beta_{\min}^{(k)} = 2 \min \{ \beta_i^{(k)} \}$ and $\beta_{\max}^{(k)} = 2 \max \{ \beta_i^{(k)} \}$.

Finally, the updating scheme of the OC method is given as

$$\tilde{\beta}_i^{(k+1)} = \begin{cases} \max\left\{(1-m)\tilde{\beta}_i^{(k)}, \tilde{\beta}_{\min}^{(k)}\right\}, & \text{if } (D_i^{(k)})^{\zeta} \tilde{\beta}_i^{(k)} \leq \max\left\{(1-m)\tilde{\beta}_i^{(k)}, \tilde{\beta}_{\min}^{(k)}\right\} \\ (D_i^{(k)})^{\zeta} \tilde{\beta}_i^{(k)}, & \text{if } \begin{cases} \max\left\{(1-m)\tilde{\beta}_i^{(k)}, \tilde{\beta}_{\min}^{(k)}\right\} < (D_i^{(k)})^{\zeta} \tilde{\beta}_i^{(k)} \\ < \min\left\{(1+m)\tilde{\beta}_i^{(k)}, \tilde{\beta}_{\max}^{(k)}\right\} \end{cases} \\ \min\left\{(1+m)\tilde{\beta}_i^{(k)}, \tilde{\beta}_{\max}^{(k)}\right\}, & \text{if } (D_i^{(k)})^{\zeta} \tilde{\beta}_i^{(k)} \geq \min\left\{(1+m)\tilde{\beta}_i^{(k)}, \tilde{\beta}_{\max}^{(k)}\right\} \end{cases} \quad (46)$$

where $\tilde{\beta}_i^{(k)}$, $\tilde{\beta}_{\min}^{(k)}$ and $\tilde{\beta}_{\max}^{(k)}$ are the regularized design variable and lateral limits ranging from 0 to 1. ζ is the damping factor and m is the move limit. Other more detailed description about the OC method can be referred to the work by Luo et al. (2008).

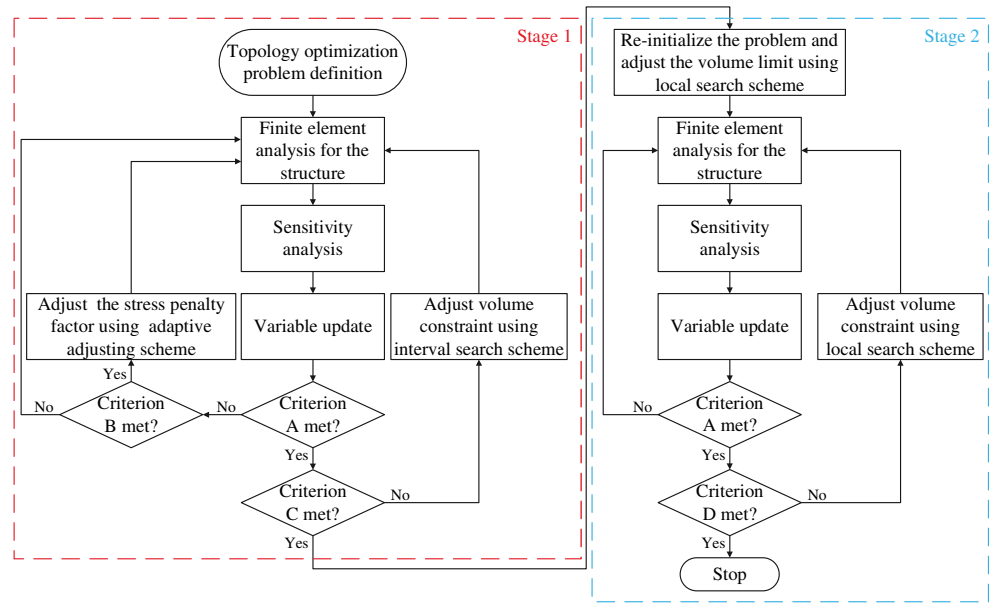
2.3.5 Solving process of stress-constrained topology optimization for minimizing the structural volume-compliance

In this paper, the original stress-constrained topology optimization for minimizing the structural volume-compliance is transformed into a stress-penalty-based compliance minimization problem and a volume-decision problem according to the method based on AVC and stress penalty. Stress penalty is considered in the objective function and used to control the local stress level of the structure in the stress-penalty-based compliance minimization problem. The combination scheme of the interval search and local search is proposed to solve the volume-decision problem. Figure 1 illustrates the flowchart of the method based on AVC and stress penalty for solving the stress-constrained volume-compliance minimization problem. As seen in Fig. 1, it can be observed that the whole solving process consists of two stages. For a succinct representation, a jointly introduction is presented as follows. The interval search scheme is used in stage 1 from Step 1 to Step 9, and the local search scheme is employed in stage 2 from Step 10 to Step 16.

- Step 1: Define the topology optimization problem, including the definition of the design domain, loading and boundary conditions. Set an allowable stress limit and an initial volume constraint, and initialized the design structure.
- Step 2: Carry out the finite element analysis for the current structure. Calculate and record the compliance and the maximum stress of the optimized structure in the current iteration.
- Step 3: Calculate the derivatives of the objective function and the volume constraints over expansion coefficients by using (27) and (28).

- Step 4: Update the expansion coefficients and the level set function according to the OC method.
- Step 5: If the terminal condition (Criterion A) for the PLSM based on CSRBFs in (29) is met or the maximum number of iterations after each change of the volume constraint is reached, record the relevant data about the current structure and go to Step 8; otherwise, go to the next step.
- Step 6: If the criteria (Criterion B) for the adaptive adjusting scheme of the stress penalty factor in (35) is satisfied, go to the next step; otherwise, go back to Step 2.
- Step 7: Adjust the stress penalty factor by using the adaptive adjusting scheme in (35) and go back to Step 2.
- Step 8: If the terminal condition (Criterion C) of the interval search scheme in (32) is not satisfied, go to the next step; otherwise, go to Step 10.
- Step 9: Adjust the volume fraction limit by using the interval search scheme in (31) and go back to Step 2.
- Step 10: Re-initialize the topology optimization problem as the one when the volume fraction limit is equal to the upper bound of the current volume fraction interval. Accordingly, all the data and the structure are reset to the corresponding ones recorded in the Step 5. Then adjust the volume fraction limit by using the local search scheme in (33).
- Step 11: Carry out the finite element analysis for the current structure. Calculate and record the compliance and the maximum stress of the optimized structure in the current iteration.
- Step 12: Calculate the derivatives of the objective function and the volume constraints over expansion coefficients by using (27) and (28).
- Step 13: Update the expansion coefficients and the level set function according to the OC method.
- Step 14: If the terminal condition (Criterion A) in (29) is met or the maximum number of iterations after each change of the volume constraint is reached, go to the next step; otherwise, go back to Step 11.

Fig. 1 Flowchart of the method based on AVC and stress penalty for solving the stress-constrained topology optimization



Step 15: If the terminal condition (Criterion D) of the local search scheme in (34) is not satisfied, go to the next step; otherwise, stop and the optimal topological structure is obtained.

Step 16: Adjust the volume fraction limit by using the local search scheme in (33) and go back to Step 11;

It can be seen from Fig. 1 that Steps 2–5 and 11–14 are used to solve the stress-penalty-based compliance minimization problem in (6), while the interval search scheme and the local search scheme are conducted with Steps 8–9 and Steps 15–16 to deal with the volume-decision problem in (30), respectively.

3 Numerical examples

In this section, numerical examples are shown to demonstrate the validity and effectiveness of the proposed method for the stress-constrained volume-compliance minimization problem. Meanwhile, the effects of the stress penalty factor, the different value Δ_{obj} and the allowable stress $\bar{\sigma}$ on the optimization results are analyzed and discussed. For all the examples, the Young’s elasticity modulus is 200GPa for solid materials and 0.001 for void materials. The Poisson’s ratio is 0.3. Additionally, the large stresses in the vicinity around the points of the concentrated forces are ignored in the stress measure.

3.1 L-shape beam

The topology optimization of a 2D L-shape beam shown in Fig. 2 is selected to verify the validity of the proposed method.

A mesh of 100×100 elements for the L-shape beam is employed. The top of the structure is fixed, and a concentrated force $F = 200\text{kN}$ is loaded at the top position of the structural right side. In this example, the initial volume fraction limit $\bar{V}^0 = 0.5$. The allowable stress is set to 130 MPa. The adaptive adjusting scheme of the stress penalty factor is conducted with the initial stress penalty factor $\alpha_0 = 5$. The different value Δ_{obj} are set to 5. ζ is set to 99% in (34) for the terminal condition of the local search scheme.

According to the method based on AVC and stress penalty, the stress-constrained volume-compliance minimization problem of the L-shape beam can be transformed into two problems: the stress-penalty-based compliance minimization problem and a volume-decision problem. According to (6), the stress-penalty-based compliance minimization problem of the L-shape beam can be formulated. By using the combination scheme of the interval search and local search, the volume-decision problem

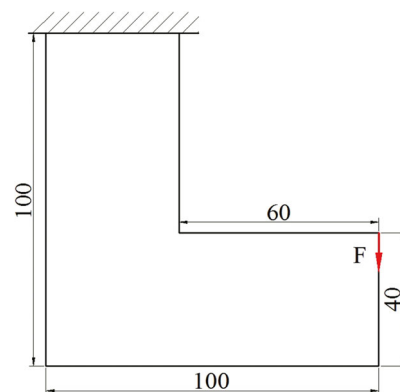


Fig. 2 Design domain of the L-shape beam

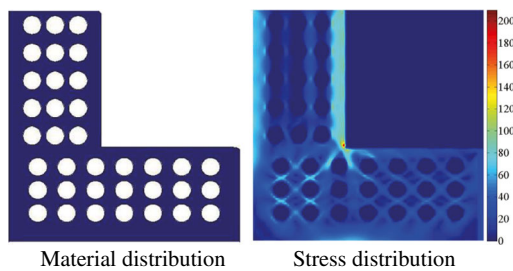


Fig. 3 Material and stress distributions for the initial configuration of the L-shape beam

can be solved. According to the solving process shown in Fig. 1, the optimal structure of the L-shape beam is obtained. The initial configuration of the L-shape beam for the optimization is given in Fig. 3. Figure 4 illustrates the intermediate designs, optimal design and their corresponding maps of the von Mises stress. The convergence histories of the objective function, volume fraction, compliance and maximum stress are shown in Fig. 5.

From Fig. 4, it can be found that the structures with smooth and clear boundaries are obtained during the optimization due to the application of the PLSM. As seen in Fig. 5(b), the volume fraction limit value is reduced at several iterations after the implementation of the interval search and local search schemes. Then, the solid materials in the structure need to be removed to satisfy the volume constraint, which causes the objective, compliance and maximum stress increase rapidly at these iterations (as seen in Fig. 5(a), 5(c) and 5 (d)). When the volume fraction limit $\bar{V}^2 = 0.3$, the maximum stress of the structure is 115.15 MPa at the 455th iteration. While the maximum stress

of the structure with the volume fraction limit $\bar{V}^3 = 0.2$ is 151.75 MPa at the 607th iteration, which is larger than the allowable stress. Thus, the volume interval search in Stage 1 of the proposed method is finished after 607 iterations, and the suitable volume fraction interval is determined as $[0, 0.3]$. Then the topology optimization problem is re-initialized as the one when the volume fraction limit is equal to 0.3, which causes the abrupt increase of the volume fraction at the 608th iteration in Fig. 5(b). The optimal structure is generated after the following 301 iterations by using the volume local search in Stage 2 of the proposed method. The compliance of the optimal structure is 41,096.27 and its maximum stress is 129.71 MPa, which meets the stress constraint. The optimal volume fraction is 0.17426. Compared with the initial volume fraction limit $\bar{V}^0 = 0.5$, the volume fraction is decreased by more than 60%. Hence, it is illustrated that the stress-constrained volume-compliance minimization problem can be effectively solved by the proposed method. A lightweight structure that meets the stress constraint is obtained and its compliance is simultaneously optimized.

Comparatively, without considering the stress constraint and the stress penalty, i.e., $\alpha = 0$ in (6), the topology optimization for minimizing the compliance of the L-shape beam with the unchanged volume fraction limit $\bar{V} = 0.5$ is presented to demonstrate the effectiveness of stress penalty in (6) on controlling the local stress level. Its optimal design is shown in Fig. 6. The maximum stress is 156.90 MPa and appears at the inner corner of the structure with the stress concentration. While as shown in Fig. 4(a), the design with the volume fraction limit $\bar{V}^0 = 0.5$ after 151 iterations by the proposed method with stress penalty has a quite different structure, especially

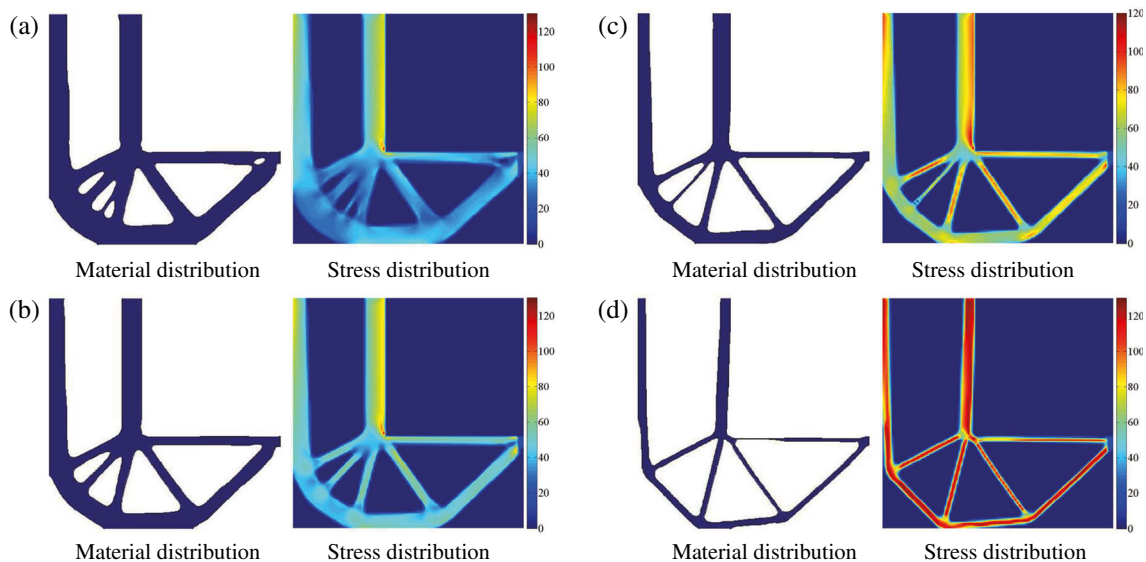
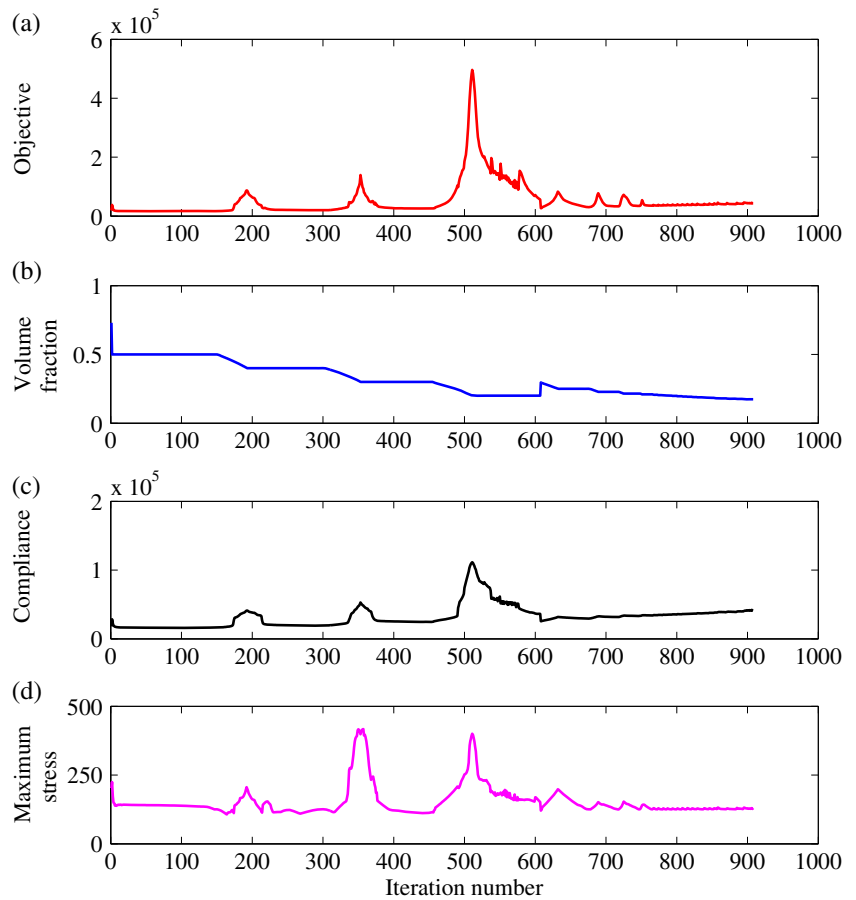


Fig. 4 Material and stress distributions for the stress-constrained volume-compliance minimization problem of the L-shape beam at different iterations: (a) step 151 with volume fraction limit $\bar{V}^0 = 0.5$; (b) step 303 with volume

fraction limit $\bar{V}^1 = 0.4$; (c) step 455 with volume fraction limit $\bar{V}^2 = 0.3$; (d) step 908 with the final volume fraction limit $\bar{V} = 0.17426$ (the optimal design)

Fig. 5 Iterative histories for the stress-constrained volume-compliance minimization problem of the L-shape beam: (a) objective; (b) volume fraction; (c) compliance; (d) maximum stress



at the inner corner of the L-shape beam. Its maximum stress is 125.14 MPa, which is lower than the allowable stress. Thus, it is demonstrated that stress penalty in (6) can effectively control the stress level when $\alpha > 0$.

3.1.1 Effects of the stress penalty factor on optimization results

To analyze the effects of the stress penalty factor on optimization results, the stress-constrained volume-compliance minimization problem of the L-shape beam is further solved under different stress penalty factors without the adaptive adjusting

scheme. Comparison of optimization results is given in Table 1.

When $\alpha = 0$ in (6), the topology optimization of the L-shape beam is conducted to obtain a structure with the minimum compliance, and it do not have the ability to control the local stress level. As α increases, the compliance will increase due to the change of the structure with the minimum compliance. While the maximum stress will decrease because stress penalty is gradually enhanced and the local stress level can be effectively controlled till the stress constraint is satisfied. Therefore, if α is set too small, the penalty of stresses that are larger than the allowable stress is not enough and the maximum stress will be still larger than the allowable stress. Then, the volume fraction limit is increased during the volume-decision by the combination search scheme. Finally, a local optimal design will be obtained. It can be seen from Table 1 that an appropriate design cannot be obtained when $\alpha = 5$. This is because sometimes more usage of materials may induce more severe stress concentration (Guo et al. 2014). Namely, even though the volume is increased during the optimization, the stress concentration still exists at the inner corner of the L-shape beam and the maximum stress is larger than the allowable stress. When $\alpha = 10$, a better design is obtained, which is close to the design obtained by the proposed method

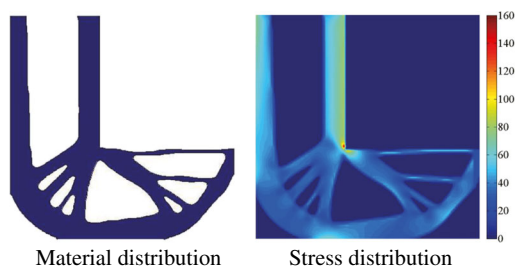
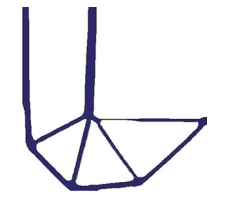

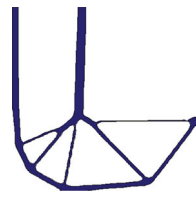
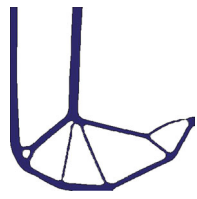
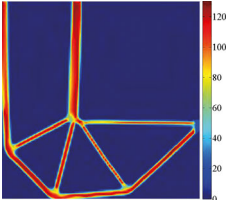
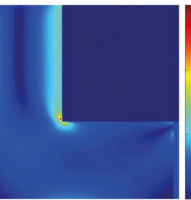
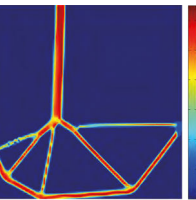
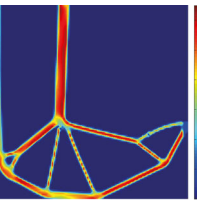


Fig. 6 Material and stress distributions for the compliance minimization problem of the L-shape beam with the unchanged volume fraction limit $\bar{V} = 0.5$

Table 1 Comparison of optimization results obtained by the proposed method for the L-shape beam under different stress penalty factors

Optimal results	Adaptive α ($\alpha_0=5$)	$\alpha=5$	$\alpha=10$	$\alpha=15$
Volume fraction	0.17426	1.0000	0.17405	0.20527
Compliance	41096.27	11484.19	42078.14	39238.62
Maximum stress (MPa)	129.71	148.39	129.92	129.23
Material distribution				
Stress distribution				

with the adaptive adjusting scheme of α . The stress constraint is satisfied. Nevertheless, the compliance is a little larger. When $\alpha = 15$, though the stress constraint is met, the final volume fraction limit is larger than the ones when the adaptive adjusting scheme of α is conducted and $\alpha = 10$. Figure 7 gives the structure obtained by the proposed method with $\alpha = 15$ at the 127th iteration under the current volume fraction limit $\bar{V}^0 = 0.5$. Compared with the optimal structure shown in Fig. 6, it can be found that the stress penalty factor ($\alpha = 15$) makes a great change of the structure at the beginning of the optimization to prevent the stress concentration, particularly at the inner corner of the L-shape beam, and then these structural characteristics will be retained in the final design. Additionally, if α is set too large, the optimization will be unstable due to the abrupt change of the objective function,

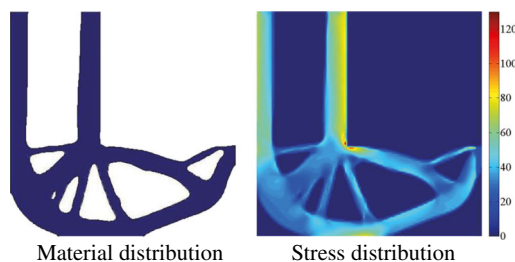


Fig. 7 Material and stress distributions for the stress-constrained volume-compliance minimization problem of the L-shape beam at the 127th iteration with the unchanged stress penalty factor $\alpha = 15$ and current volume fraction limit $\bar{V}^0 = 0.5$

and then a local optimum will be easily obtained. Therefore, it is demonstrated that the adaptive adjusting scheme of the stress penalty factor is effective.

3.1.2 Effects of the Δ_{obj} on optimization results

To analyze the effects of Δ_{obj} in (7) and (8) on optimization results, the stress-constrained volume-compliance minimization problem of the L-shape beam is further solved under different values of Δ_{obj} . In order to make sure there is only one parameter for discussion, the adaptive adjusting scheme of the stress penalty factor is not applied and α is set to 10. Comparison of optimization results is given in Table 2.

Δ_{obj} controls the width of the transition band of the Heaviside function in stress penalty, and an inappropriate Δ_{obj} may cause the violation of the stress constraint. If it is set too small, the objective function in (10) and its sensitivity in (27) will be nearly equivalent to the discontinuous functions, which will lead to the great abrupt change of the penalty item and the generation of a local optimum during the optimization. For example, set $\Delta_{obj} = 1$, the structure obtained by the proposed method at the 46th with the volume fraction limit $\bar{V}^0 = 0.5$ is given in Fig. 8(a). Its maximum stress is 133.86 MPa and larger than the allowable stress. Actually, this structure is a local optimum because it can be found from Fig. 4(a) that the maximum stress of the L-shape beam with the volume fraction limit $\bar{V}^0 = 0.5$ can be lower than the allowable stress. Then the volume fraction limit should be

Table 2 Comparison of optimization results obtained by the proposed method for the L-shape beam under different Δ_{obj} and $\alpha = 10$

Optimal results	$\Delta_{obj}=1$	$\Delta_{obj}=5$	$\Delta_{obj}=10$	$\Delta_{obj}=120$
Volume fraction	0.19913	0.17405	0.17912	1.0000
Compliance	35636.67	42078.14	42757.52	11484.19
Maximum stress (MPa)	129.07	129.92	129.60	148.39
Material distribution				
Stress distribution				

increased to 0.6. The structure obtained by the proposed method with $\Delta_{obj} = 1$ at the 198th iteration with the volume fraction limit $\bar{V}^1 = 0.6$ is given in Fig. 8(b). Its maximum stress is 128.30 MPa, lower than the allowable stress. Accordingly, the volume interval search in Stage 1 of the proposed method is finished, and the volume local search is conducted. From the results with $\Delta_{obj} = 1$ in Table 2, it can be seen that an acceptable design with the optimal volume fraction 0.19913 is obtained due to the continual change of the volume fraction limit by the local search scheme. Therefore, the proposed combination search scheme for volume-decision is helpful in avoiding a local optimum to some degree. On the other hand, if Δ_{obj} is set relatively large, such as 5 and 10, the penalty item will become smoother in the neighborhood around the stress point where the stress value is equal to the allowable value. From Table 2, it can be observed that good designs can be obtained when Δ_{obj} is set to 5 and 10. However, Δ_{obj} should not be set too large, otherwise (6) will

be nearly equivalent to the compliance minimization topology optimization problem and the stress level cannot be effectively controlled. From Table 2, it can be found that an appropriate design cannot be obtained when $\Delta_{obj} = 120$. The stress constraint is not satisfied without the effective control of the stress level. Therefore, the drawback of the proposed method is that a suitable value of Δ_{obj} in stress penalty needs to be predetermined by the designers according to the specific optimization problems and their design experience.

3.1.3 Effects of the allowable stress on optimization results

To analyze the effects of the allowable stress on optimization results, the stress-constrained volume-compliance minimization problem of the L-shape beam is further solved under different allowable stresses. During the optimization, the adaptive adjusting scheme of the stress penalty factor is

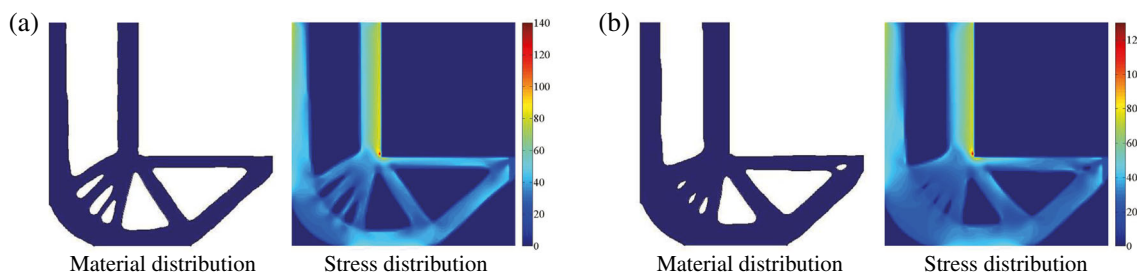
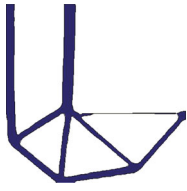
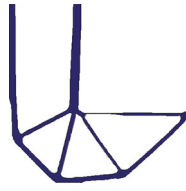
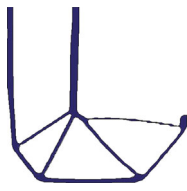
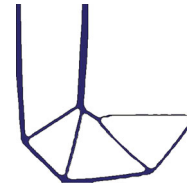
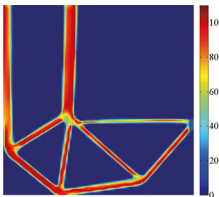
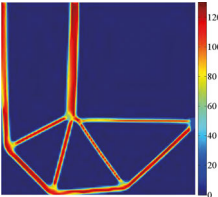
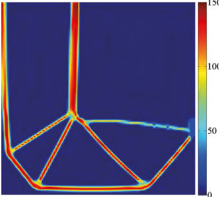
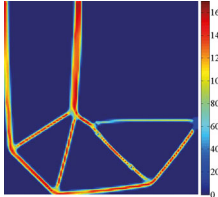


Fig. 8 Material and stress distributions for the stress-constrained volume-compliance minimization problem of the L-shape beam with $\Delta_{obj} = 1$ at different iterations: (a) step 46 with volume fraction limit $\bar{V}^0 = 0.5$; (b) step 198 with volume fraction limit $\bar{V}^1 = 0.6$

Table 3 Comparison of optimization results obtained by the proposed method for the L-shape beam under different allowable stresses

Optimal results	$\bar{\sigma} = 110\text{MPa}$	$\bar{\sigma} = 130\text{MPa}$	$\bar{\sigma} = 150\text{MPa}$	$\bar{\sigma} = 170\text{MPa}$
Volume fraction	0.22169	0.17426	0.14767	0.13164
Compliance	40561.80	41096.27	51761.49	51485.95
Maximum stress (MPa)	109.24	129.71	149.43	169.71
Material distribution				
Stress distribution				

conducted and Δ_{obj} is set to 5. Comparison of optimization results is given in Table 3.

From Table 3, it can be seen that all the problems under different allowable stresses can be solved by the proposed method. As the allowable stress increases, the final volume of the L-shape beam is reduced. Due to the compliance-based term in the objective function in (6), the structural compliance is optimized to exclude the pathological structures with small stiffness. From the material distributions in Table 2, it can be observed that the optimal designs under different allowable stresses have the same topological structure. It is worth noting that when the allowable stress is set to 170 MPa, stress penalty is not always active at the beginning of the optimization because the maximum stress of the structure with the initial volume fraction limit $\bar{V}^0 = 0.5$ is lower than 170 MPa, which can be inferred from the stress distribution in Fig. 6. As the volume fraction limit decreases, the maximum stress is increased and stress penalty becomes active. Through the proposed method, a lightweight design that meets the stress constraint is obtained, and its compliance is simultaneously optimized.

3.1.4 Effects of the initial structural configuration on optimization results

To analyze the effects of the initial configuration on optimization results, the stress-constrained volume-compliance

minimization problem of the L-shape beam is further solved under different initial configurations. Compared with the initial configuration in Fig. 3, two different initial configurations A and B are employed and shown in Fig. 9. All the parameters have the same values as those for the initial configuration in Fig. 3 and its corresponding optimization in Fig. 4. The intermediate designs, optimal design and their corresponding maps of the von Mises stress are given in Figs. 10 and 11, respectively.

As seen in Fig. 10, under the initial configuration A, the final design is obtained after 993 iterations. The compliance, volume fraction and maximum stress of the optimal structure are 41,627.39, 0.17998 and 129.57 MPa, respectively. As shown in Fig. 11, under the initial configuration B, the final design is obtained after 1350 iteration. The compliance, volume fraction and maximum stress of the optimal structure are 39,326.22, 0.20635 and 129.95 MPa, respectively. From Figs. 4, 10 and 11, it can be found that the structural topologies of the intermediate designs are different, but the structural topologies of the final designs are the same under three different initial configurations. For the three final designs, their shapes are a little different, which lead to different structural performances. However, their compliances, volume fractions and maximum stresses are close. Besides, all their structural volumes decrease largely and all the stress constraints are satisfied. It means lightweight designs, which meets the stress constraint and whose compliance is simultaneously optimized, can be obtained under different initial configurations

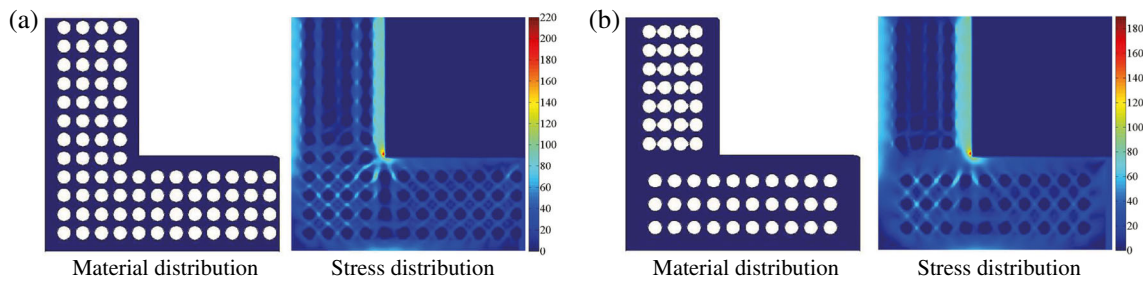


Fig. 9 Material and stress distributions for two different initial configurations of the L-shape beam: (a) initial configuration A; (b) initial configuration B

by the proposed method. Therefore, the results show that, to some extent, the proposed method can alleviate the problem of dependency of the initial configuration which is the inherent problem of the PLSM (Luo et al. 2008).

3.1.5 Different loading condition for the L-shape beam

For the L-shape beam shown in Fig. 2, the stress-constrained volume-compliance minimization problem is studied when the concentrated force F is loaded at the middle point of the structural right side (seen in Fig. 12). The values of all the parameters are not changed. The initial volume fraction limit $\bar{V}^0 = 0.5$ and the initial configuration of the L-shape beam in Fig. 3 is also employed in this example. Figure 13 shows the corresponding initial stress distribution. The proposed method are used to deal with this problem. Figure 14 illustrates the intermediate designs, optimal design and their corresponding stress distributions. The convergence histories of the objective, volume fraction, compliance and maximum stress are shown in Fig. 15.

From Fig. 15, it can be observed that the compliance and maximum stress change rapidly after each change of the volume fraction limit constraint, leading to the oscillation of the iterative curves. After 645 iterations, the volume interval search in Stage 1 of the proposed method is finished. The optimal structure is generated after the following 763 iterations by the volume local search in Stage 2 of the proposed method. The compliance of the optimal structure shown in Fig. 14(d) is 41,807.28 and its maximum stress is 129.65 MPa which meets the stress constraint. The optimal volume fraction is 0.17866. Compared with the initial volume fraction limit $\bar{V}^0 = 0.5$, the volume fraction is decreased by more than 60%. In order to further verify the effectiveness of stress penalty in the (6), we conduct the compliance minimization topology optimization (namely $\alpha = 0$ in (6)) for the L-shape beam under this load case with the unchanged volume fraction limit $\bar{V} = 0.5$. Its optimal design and the corresponding stress distribution are shown in Fig. 16. It can be seen that there is stress concentration at the inner corner. The maximum stress is 158.63 MPa, more than the allowable stress. Compared with this design, the structure obtained by the

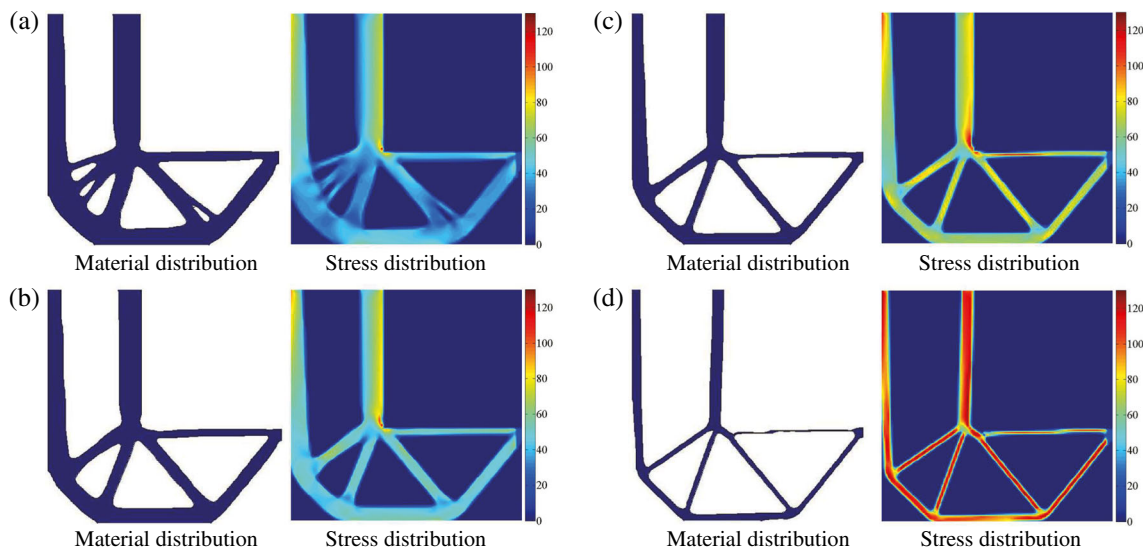


Fig. 10 Material and stress distributions for the stress-constrained volume-compliance minimization problem of the L-shape beam under initial configuration A at different iterations: (a) step 58 with volume fraction limit $\bar{V}^0 = 0.5$; (b) step 210 with volume fraction limit $\bar{V}^1 =$

0.4; (c) step 362 with volume fraction limit $\bar{V}^2 = 0.3$; (d) step 993 with the final volume fraction limit $\bar{V} = 0.17998$ (the optimal design)

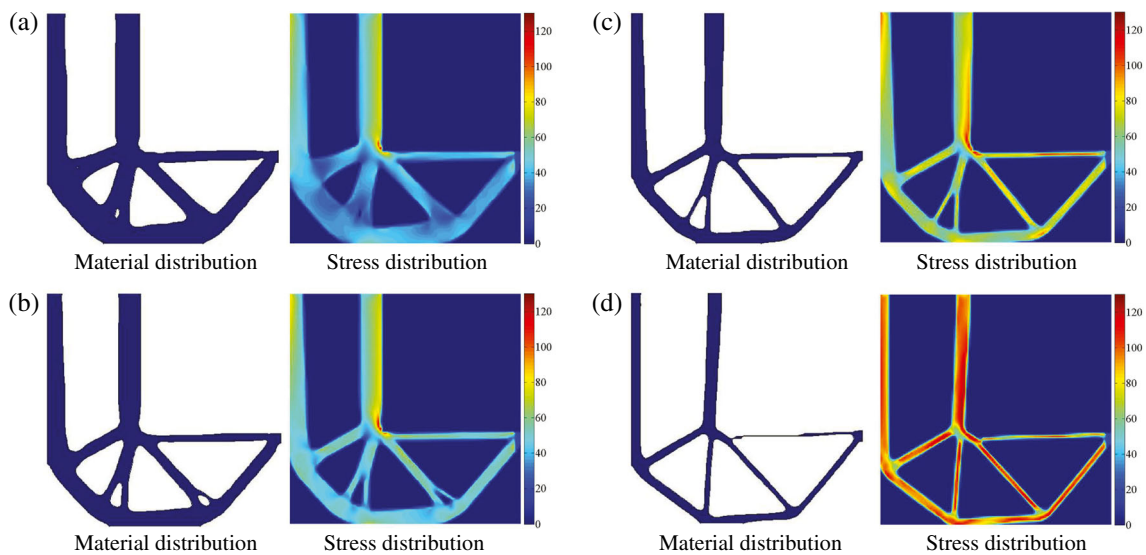


Fig. 11 Material and stress distributions for the stress-constrained volume-compliance minimization problem of the L-shape beam under initial configuration B at different iterations: (a) step 222 with volume fraction limit $\bar{V}^0 = 0.5$; (b) step 374 with volume fraction limit $\bar{V}^1 = 0.4$;

(c) step 526 with volume fraction limit $\bar{V}^2 = 0.3$; (d) step 1350 with the final volume fraction limit $\bar{V} = 0.20635$ (the optimal design)

proposed method with the volume fraction limit $\bar{V}^0 = 0.5$ in Fig. 14(a) has smoother boundary at the inner corner. The stress concentration is eliminated, and the maximum stress 125.65 MPa is lower than the allowable stress. Therefore, it is demonstrated once again that the proposed method is effective to solve the stress-constrained volume-compliance minimization problem.

3.1.6 Computational efficiency of the proposed method

The CPU cost of the proposed method is almost equal to that of solving the stress-penalty-based compliance minimization problem under the volume constraint, because solving the volume-decision problem is only a process of judgment and assignment which takes very little time. For the stress-penalty-based compliance minimization problem, stress penalty is used for the control of the local stress level, which is an added term in the objective function instead of the constraints. This can avoid a

large number of finite element constraints in conventional local methods for controlling the stress level. On the other hand, the CPU time per iteration of the stress-penalty-based compliance minimization optimization under the volume constraint is close to that of the global stress method. For example, for the L-shape beam in Fig. 2, on average, the proposed method takes 18.55 s per iteration, while the global stress method (i.e., the p -norm method) takes 17.63 s per iteration. Therefore, the proposed method combines the advantages of the local and global stress methods, namely the effective control of the local stress level and the high solving efficiency. However, during solving the stress-constrained topology optimization of minimizing the structural volume-compliance by the proposed method, the volume constraint needs to be constantly adjusted to find an appropriate volume fraction limit, which leads to more iterations. Nevertheless, compared with the local stress method, when a great number of finite elements are involved during the optimization, the proposed method may take a lower CPU cost for the whole solving process. Under this case, the effect of the iterations on the CPU cost is smaller than that of the number of finite elements.

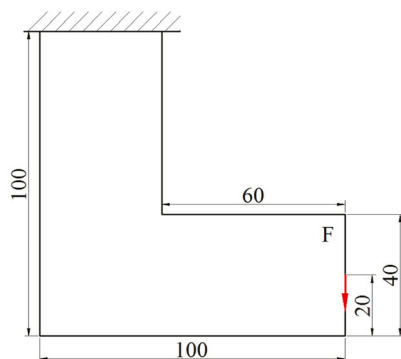


Fig. 12 L-shape beam under another load case

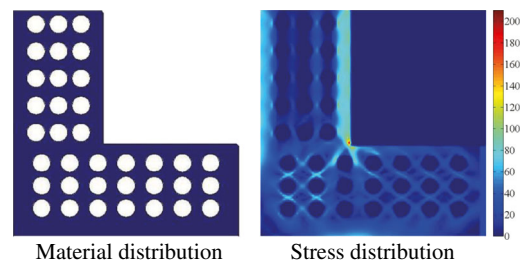


Fig. 13 Material and stress distributions for the initial configuration of the L-shape beam under another load case

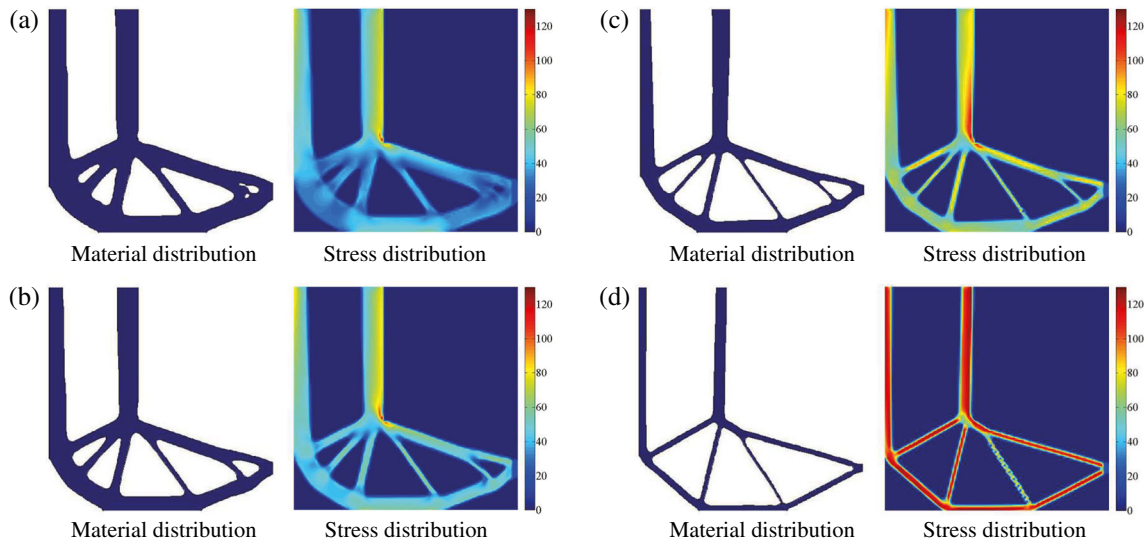


Fig. 14 Material and stress distributions for the stress-constrained volume-compliance minimization problem of the L-shape beam at different iterations under another load case: **(a)** step 229 with volume fraction limit $\bar{V}^0 = 0.5$; **(b)** step 343 with volume fraction limit $\bar{V}^1 =$

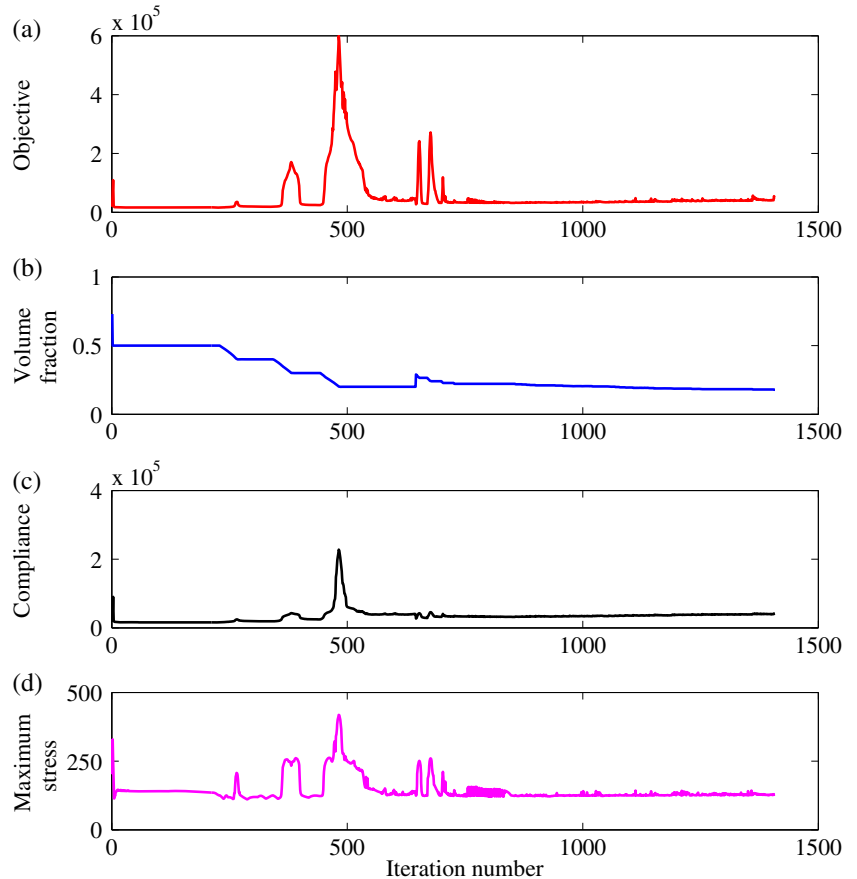
0.4; **(c)** step 443 with volume fraction limit $\bar{V}^2 = 0.3$; **(d)** step 1408 with final volume fraction limit $\bar{V} = 0.17866$ (the optimal design)

3.2 Squared plate

In this section, the topology optimization of a 2D squared plate shown in Fig. 17 is selected to verify the effectiveness

of the proposed method. This example emulates the fracture mode I of a squared plate with length $L_1 = 80$ and fracture length $L_2 = 40$. A concentrated force is applied to open the fracture, which produces high stresses at the fracture tip (Jr

Fig. 15 Iterative histories for the stress-constrained volume-compliance minimization problem of the L-shape beam under another load case: **(a)** objective; **(b)** volume fraction; **(c)** compliance; **(d)** maximum stress



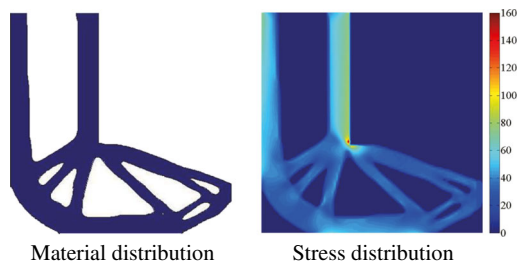


Fig. 16 Material and stress distributions for the compliance minimization problem of the L-shape beam under another load case with the unchanged volume fraction limit $\bar{V} = 0.5$

Emmendoerfer and Fancello 2014). A mesh of 80×80 elements for the squared plate is employed, but only the right symmetric part of the plate was applied with a mesh of 40×80 elements in the optimization due to the symmetry of the structure. In this example, the initial volume fraction limit $\bar{V}^0 = 0.4$. The allowable stress is set to 130 MPa. The adaptive adjusting scheme of the stress penalty factor is conducted with the initial stress penalty factor $\alpha_0 = 5$, and the different value Δ_{obj} is set to 5. ζ is set to 99% in (34) for the terminal condition of the local search scheme.

To provide a reference for the stress-constrained volume-compliance minimization topology optimization, the compliance minimization topology optimization is conducted for this squared plate with the unchanged volume fraction limit $\bar{V} = 0.4$. The initial configuration of the squared plate for the optimization is given in Fig. 18. Figure 19 shows the optimal design with the minimum compliance. It can be seen that stress concentration exists and high stresses appear at the fracture tip. The maximum stress is 173.69 MPa, which is more than the allowable stress.

In the following, the stress-constrained volume-compliance minimization problem of the squared plate is solved by the proposed method according to the solving process in Fig. 1. The initial structural configuration in Fig. 18 is employed. Figure 20 illustrates the intermediate designs, optimal design and their corresponding stress distributions. The convergence

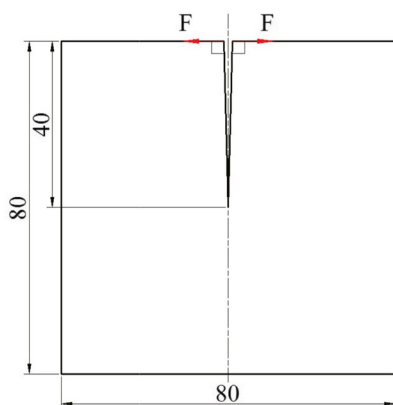


Fig. 17 Design domain of the squared plate

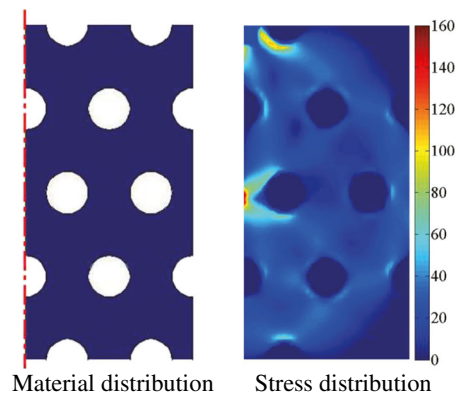


Fig. 18 Material and stress distributions for the initial configuration of the squared plate

histories of the objective function, volume fraction, compliance and maximum stress are shown in Fig. 21.

As shown in Fig. 21, the oscillation of the iterative curves exists during the optimization around the 400-600th iterations. This is because the current volume fraction limit is too small, causing the instability during the optimization. The Stage 1 in the proposed method to search a suitable volume interval is finished after 621 iterations. Then, the topology optimization problem is re-initialized and the volume constraint is reset for the local search scheme. The instability of the optimization is avoided, and the optimal structure with smooth and clear boundaries is obtained after 795 iterations. The final compliance is 17,856.39 and the final volume fraction is 0.17139. The volume of the squared plate is decreased by more than 50%. Compared with the compliance minimization design shown in Fig. 19, the final design obtained by the proposed method eliminates the stress concentration at the fracture tip. Meanwhile, its maximum stress is 128.94 MPa and the stress constraint is satisfied. Thus, it is demonstrated the proposed method are effective to obtain a lightweight structure that meets the stress constraint and whose compliance is simultaneously optimized.

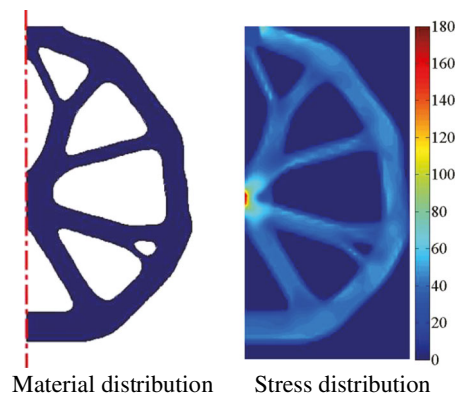


Fig. 19 Material and stress distributions for the compliance minimization problem of the squared plate with the unchanged volume fraction limit $\bar{V} = 0.4$

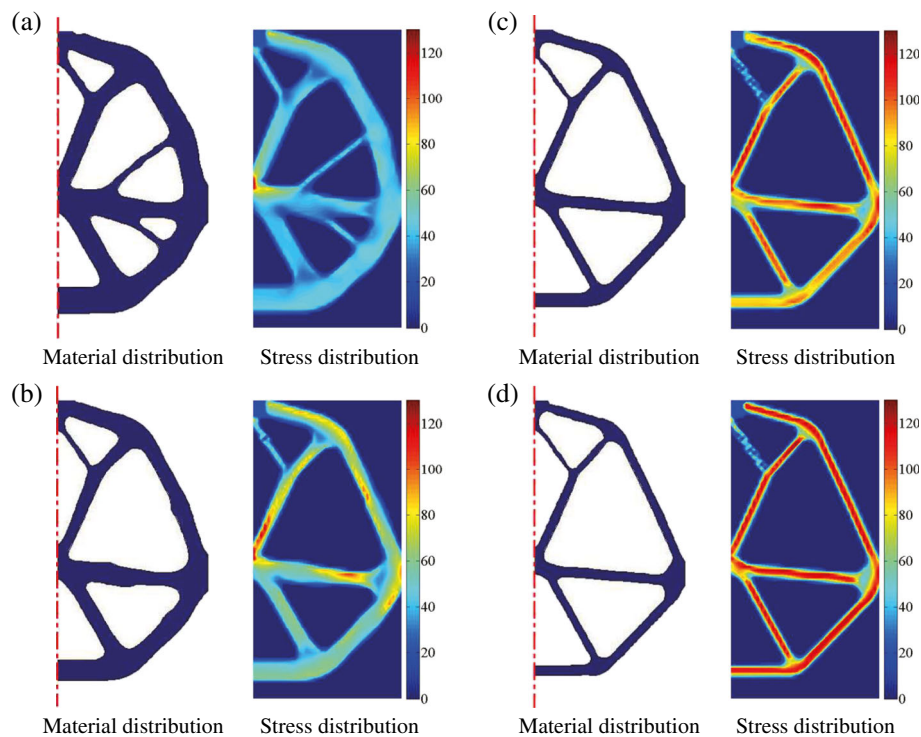


Fig. 20 Material and stress distributions for the stress-constrained volume-compliance minimization problem of the squared plate at different iterations: (a) step 112 with volume fraction limit $\bar{V}^0 = 0.4$; (b) step 177 with volume

fraction limit $\bar{V}^1 = 0.3$; (c) step 319 with volume fraction limit $\bar{V}^2 = 0.2$; (d) step 795 with the final volume fraction limit $\bar{V} = 0.17139$ (the optimal design)

3.3 Two-bar truss

In this section, the topology optimization of a 2D two-bar truss shown in Fig. 22 is chosen to verify the effectiveness of the proposed method in case of the optimal design with no stress concentrations. A mesh of 40×80 elements for the two-bar truss is employed. The left side of the structure is fixed, and a concentrated force $F = 400\text{kN}$ is loaded at the middle position of the structural right side. In this example, the initial volume fraction limit $\bar{V}^0 = 0.3$. The allowable stress is set to 130 MPa. The adaptive adjusting scheme of the stress penalty factor is conducted with the initial stress penalty factor $\alpha_0 = 5$. The different value Δ_{obj} are set to 5. ζ is set to 99% in (34) for the terminal condition of the local search scheme.

The stress-constrained volume-compliance minimization problem of the two-bar truss is solved by the proposed method according to the solving process in Fig. 1. The initial structural configuration in Fig. 23 is employed. Figure 24 illustrates the intermediate designs, optimal design and their corresponding stress distributions. The convergence histories of the objective function, volume fraction, compliance and maximum stress are shown in Fig. 25.

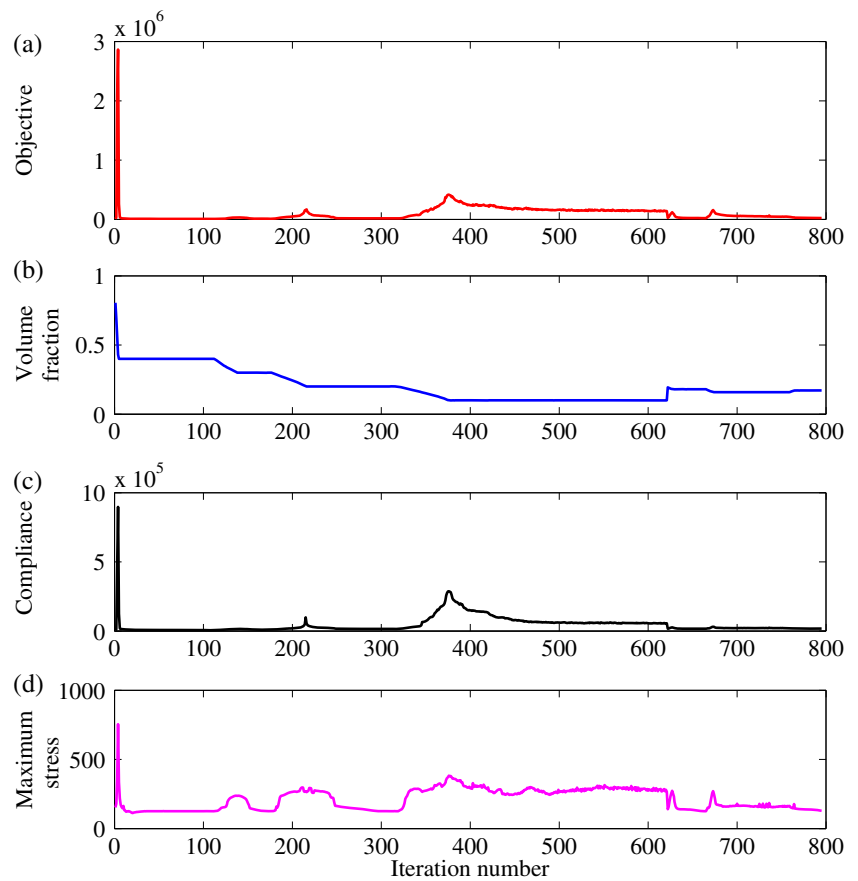
After 455 iterations, the optimal design with the minimum volume and homogeneous stress level is obtained, whose topology is the same as the one obtained by the compliance-based topology optimization. This is easily understood

because the stress design and the compliance design are almost the same when the geometric constraint is not active according to the work by Pedersen (2000). The compliance, volume fraction and maximum stress of the optimal structure are 10,189.44, 0.078125 and 129.05 MPa, respectively. The volume of the two-bar truss is decreased by more than 70%, and the stress constraint is satisfied. Therefore, it is demonstrated that the proposed method is also effective in case of the optimal design with no stress concentrations.

4 Conclusions

The research focuses on the stress-constrained topology optimization of minimizing the structural volume-compliance. A new method based on AVC and stress penalty is proposed. According to this method, the original stress-constrained volume-compliance minimization problem is transformed into two simple and related problems: the stress-penalty-based compliance minimization problem and the volume-decision problem. In the former problem, stress penalty is conducted and used for the control of the local stress level, which is considered as an added term in the objective function instead of the constraint. This can avoid a large number of finite element constraints in conventional local methods for controlling the stress level. To solve the stress-penalty-based compliance

Fig. 21 Iterative histories for the stress-constrained volume-compliance minimization problem of the squared plate: (a) objective; (b) volume fraction; (c) compliance; (d) maximum stress



minimization problem, the PLSM with CSRBFs is used. Additionally, an adaptive adjusting scheme of the stress penalty factor is employed to improve the control of the local stress level. To solve the volume-decision problem, a combination scheme of the interval search and local search is put forward. Specifically, the interval search scheme is used to narrow the search range of the feasible volume fraction limit and rapidly find a suitable volume fraction limit interval. And then the local search scheme is employed to determine the

optimal volume fraction limit which will be transferred to the stress-penalty-based compliance minimization problem. Numerical examples are presented to test the proposed method. Results indicate that by using the proposed method, a lightweight structure that meets the stress constraint can be obtained and its compliance is simultaneously optimized.

For the proposed method, two parameters (α and Δ_{obj}) have a great influence on optimization results and should be

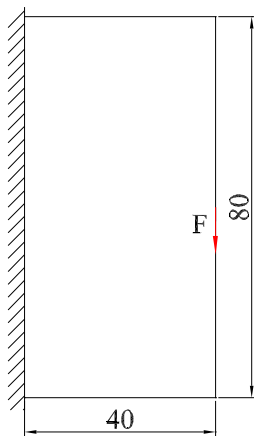


Fig. 22 Design domain of the two-bar truss

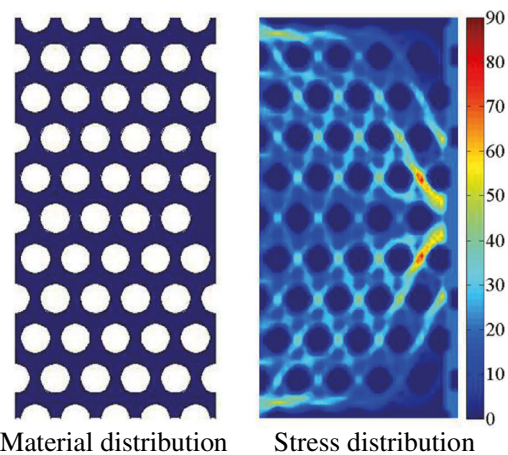


Fig. 23 Material and stress distributions for the initial configuration of the two-bar truss

Fig. 24 Material and stress distributions for the stress-constrained volume-compliance minimization problem of the two-bar truss at different iterations: (a) step 48 with volume fraction limit $\bar{V}^0 = 0.3$; (b) step 142 with volume fraction limit $\bar{V}^1 = 0.2$; (c) step 259 with volume fraction limit $\bar{V}^2 = 0.1$; (d) step 455 with the final volume fraction limit $\bar{V} = 0.078125$ (the optimal design)

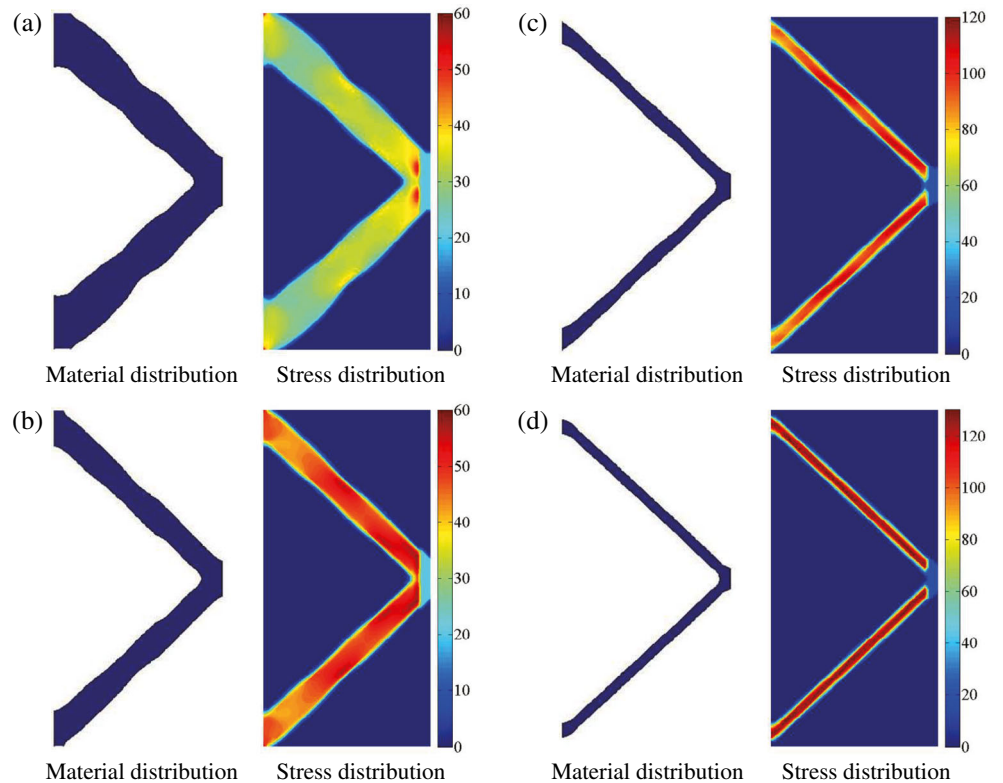
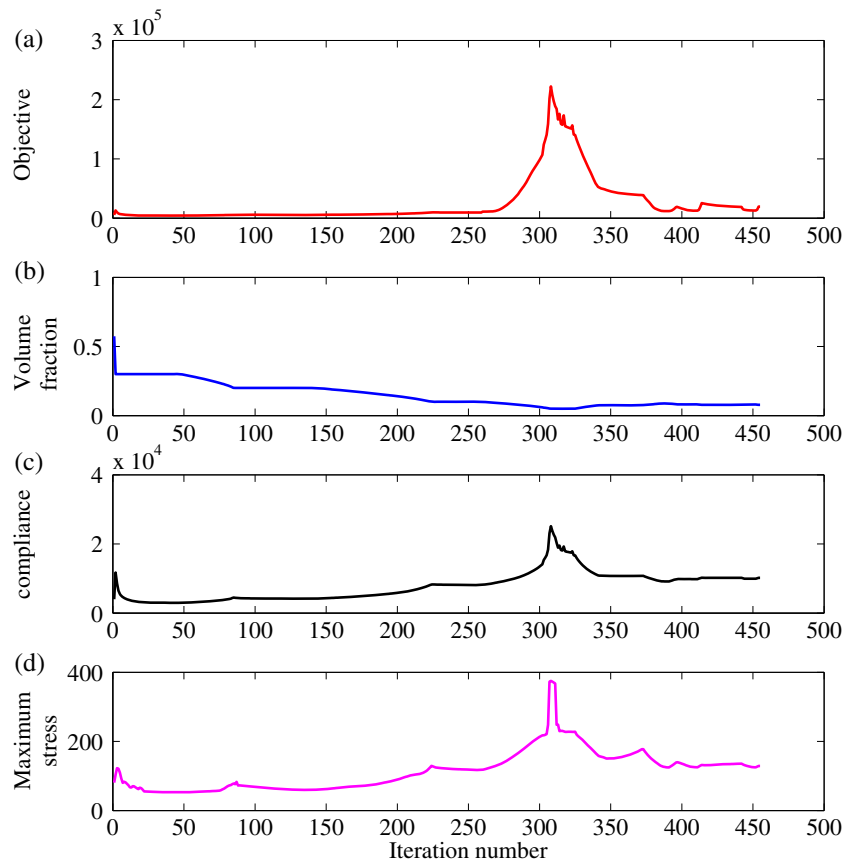


Fig. 25 Iterative histories for the stress-constrained volume-compliance minimization problem of the two-bar truss: (a) objective; (b) volume fraction; (c) compliance; (d) maximum stress



set up during the optimization, besides some necessary parameters for the PLSM, the OC method and the definition of the optimization problem, such as the radius of support, move limit and allowable stress. The adaptive adjusting scheme of the stress penalty factor is used to choose an appropriate stress penalty factor in this paper. According to the numerical experiments, the value of Δ_{obj} is suggested to be set to 2.5% to 10% of the allowable stress to ensure the stability of the optimization and obtain a good solution.

However, some shortcomings exist in the proposed method. It is worth noting that solving the volume-decision problem in (30) might be more complicated due to the nonlinear relationship between the stress level and structural volume under different structural topologies and local shapes. Though it is illustrated that the proposed method can obtain some acceptable structures in the numerical examples, the local search scheme in (33) for the volume-decision problem does not consider the above nonlinear relationship and should be improved in further work. In addition, to improve the computational efficiency, the finite element method with structured four-node bi-linear elements and the ersatz material model are used in the displacement analysis in this paper. However, it is poor to accurately describe and analyze the small local structure, especially when the structural volume becomes small and the size of small local structure is close to or even smaller than the mesh size. As part of further work, the X-FEM approaches and body-fitted adaptive mesh techniques can be used to address this problem and ensure the accuracy of the stress calculation and the computational efficiency of the FEM analysis.

Funding This research was supported by the National Basic Scientific Research Program of China [grant number JCKY2016110C012]; and the National Natural Science Foundation of China [grant numbers 51675196 51421062].

References

- Allaire G, Jouve F, Toader AM (2004) Structural optimization using sensitivity analysis and a level-set method. *J Comput Phys* 194:363–393
- Bendsøe MP (1995) *Optimization of structural topology, shape and material*. Springer, Berlin Heidelberg
- Bendsøe MP, Sigmund O (2003) *Topology optimization: theory, methods and applications*, 2nd edn. Springer, Berlin
- Bruggi M (2008) On an alternative approach to stress constraints relaxation in topology optimization. *Struct Multidiscip Optim* 36:125–141
- Bruggi M, Venini P (2008) A mixed FEM approach to stress-constrained topology optimization. *Int J Numer Methods Eng* 73:1693–1714
- Cheng GD, Guo X (1997) ϵ -Relaxed approach in structural topology optimization. *Struct Optim* 13:258–266
- Choi KK, Kim NH (2005) *Structural sensitivity analysis and optimization*. Springer, New York
- Collet M, Bruggi M, Duysinx P (2016) Topology optimization for minimum weight with compliance and simplified nominal stress constraints for fatigue resistance. *Struct Multidiscip Optim* 55:1–17
- De Leon DM, Alexandersen J, Fonseca JSO, Sigmund O (2015) Stress-constrained topology optimization for compliant mechanism design. *Struct Multidiscip Optim* 52:929–943
- Deaton JD, Grandhi RV (2014) A survey of structural and multidisciplinary continuum topology optimization: post 2000. *Struct Multidiscip Optim* 49:1–38
- Duysinx P, Bendsøe MP (1998) Topology optimization of continuum structures with local stress constraints. *Int J Numer Methods Eng* 43:1453–1478
- Duysinx P, Sigmund O (1998) New developments in handling stress constraints in optimal material distribution. In: *Proceedings of the 7th AIAA/USAF/NASA/ISSMO symposium on multidisciplinary analysis and optimization*, St. Louis, Missouri 1501–1509
- Guilherme CEM, Fonseca JSO (2007) Topology optimization of continuum structures with epsilon-relaxed stress constraints. In: Alves M, da Costa Mattos H (eds) *International symposium on solid mechanics, mechanics of solids in Brazil*, vol 1. Brazilian Society of Mechanical Sciences in Engineering 239–250
- Guo X, Zhang WS, Wang MY, Wei P (2011) Stress-related topology optimization via level set approach. *Comput Methods Appl Mech Eng* 200:3439–3452
- Guo X, Zhang W, Zhong W (2014) Stress-related topology optimization of continuum structures involving multi-phase materials. *Comput Methods Appl Mech Eng* 268:632–655
- Guo X, Zhang W, Zhang J, Yuan J (2016) Explicit structural topology optimization based on moving morphable components (MMC) with curved skeletons. *Comput Methods Appl Mech Eng* 310:711–748
- Haug EJ, Choi KK, Komkov V (1986) *Design sensitivity analysis of structural systems*. Academic Press, London
- Holmberg E, Torstenfelt B, Klarbring A (2013) Stress constrained topology optimization. *Struct Multidiscip Optim* 48:33–47
- Jeong SH, Yoon GH, Takezawa A, Choi DH (2014) Development of a novel phase-field method for local stress-based shape and topology optimization. *Comput Struct* 132:84–98
- Jr Emmendoerfer H, Fancello EA (2014) A level set approach for topology optimization with local stress constraints. *Int J Numer Methods Eng* 99:129–156
- Kaw AK, Kalu EE, Duc N (2011) *Numerical Methods with Applications*. University of South Florida, Textbooks Collection 11. http://scholarcommons.usf.edu/oa_textbooks/11
- Kiyono CY, Vatanabe SL, Silva ECN, Reddy JN (2016) A new multi-p-norm, formulation approach for stress-based topology optimization design. *Compos Struct* 156:10–19
- Lee K, Ahn K, Yoo J (2016) A novel P-norm correction method for lightweight topology optimization under maximum stress constraints. *Comput Struct* 171:18–30
- Lin CY, Sheu FM (2009) Adaptive volume constraint algorithm for stress limit-based topology optimization. *Comput Aided Des* 41:685–694
- Liu Z, Korvink JG (2008) Adaptive moving mesh level set method for structure topology optimization. *Eng Optim* 40:529–558
- Lopes CG, Novotny AA (2016) Topology design of compliant mechanisms with stress constraints based on the topological derivative concept. *Struct Multidiscip Optim* 54:737–746
- Luo Z, Tong L, Wang MY, Wang S (2007) Shape and topology optimization of compliant mechanisms using a parameterization level set method. *J Comput Phys* 227:680–705
- Luo Z, Wang MY, Wang S, Wei P (2008) A level set-based parameterization method for structural shape and topology optimization. *Int J Numer Methods Eng* 76:1–26
- Luo Y, Wang MY, Kang Z (2013) An enhanced aggregation method for topology optimization with local stress constraints. *Comput Methods Appl Mech Eng* 254:31–41
- París J, Navarrina F, Colomina I, Casteleiro M (2010) Block aggregation of stress constraints in topology optimization of structures. *Adv Eng Softw* 41:433–441

- Pedersen P (2000) On optimal shapes in materials and structures. *Struct Multidiscip Optim* 19:169–182
- Pereira JT, Fancello EA, Barcellos CS (2004) Topology optimization of continuum structures with material failure constraints. *Struct Multidiscip Optim* 26:50–66
- Qiu GY, Li XS (2010) A note on the derivation of global stress constraints. *Struct Multidiscip Optim* 40:625–628
- Rong JH, Xiao TT, Yu LH, Rong XP, Xie YJ (2016) Continuum structural topological optimizations with stress constraints based on an active constraint technique. *Int J Numer Methods Eng* 108:326–360
- Sigmund O (2001) A 99 line topology optimization code written in Matlab. *Struct Multidiscip Optim* 21:120–127
- Silva GAD, Cardoso EL (2017) Stress-based topology optimization of continuum structures under uncertainties. *Comput Methods Appl Mech Eng* 313:647–672
- Verbart A, Langelaar M, Keulen FV (2016) Damage approach: a new method for topology optimization with local stress constraints. *Struct Multidiscip Optim* 53:1081–1098
- Wang MY, Wang X (2004) PDE-driven level sets, shape sensitivity and curvature flow for structural topology optimization. *Comput Model Eng Sci* 6:373–395
- Wang MY, Wang X, Guo D (2003) A level set method for structural topology optimization. *Comput Methods Appl Mech Eng* 192:227–246
- Wang Y, Luo Z, Kang Z, Zhang N (2015) A multi-material level set-based topology and shape optimization method. *Comput Methods Appl Mech Eng* 283:1570–1586
- Wendland H (1995) Piecewise polynomial, positive definite and compactly supported radial functions of minimal degree. *Adv Comput Math* 4:389–396
- Xia Q, Shi T, Liu S, Wang MY (2012) A level set solution to the stress-based structural shape and topology optimization. *Comput Struct* 90–91:55–64
- Yang RJ, Chen CJ (1996) Stress-based topology optimization. *Struct Multidiscip Optim* 12:98–105
- Yoon GH (2014) Stress-based topology optimization method for steady-state fluid–structure interaction problems. *Comput Methods Appl Mech Eng* 278:499–523
- Zhang W, Yuan J, Zhang J, Guo X (2015) A new topology optimization approach based on moving Morphable components (MMC) and the ersatz material model. *Struct Multidiscip Optim* 53:1243–1260